

# Confinement, Holonomy and Correlated Instanton-Dyon Ensemble I: SU(2) Yang-Mills Theory

Miguel Angel Lopez-Ruiz<sup>a</sup>, Yin Jiang<sup>a</sup>, Jinfeng Liao<sup>a</sup>

<sup>a</sup>*Physics Department and Center for Exploration of Energy and Matter, Indiana University,  
2401 N Milo B. Sampson Lane, Bloomington, IN 47408, USA*

---

## Abstract

The mechanism of confinement in Yang-Mills theories remains a challenge to our understanding of nonperturbative gauge dynamics. While it is widely perceived that confinement may arise from chromo-magnetically charged gauge configurations with nontrivial topology, it is not clear what types of configurations could do that and how, in pure Yang-Mills and QCD-like (non-supersymmetric) theories. Recently a promising approach has emerged, based on statistical ensembles of dyons/anti-dyons that are constituents of instanton/anti-instanton solutions with nontrivial holonomy where the holonomy plays a vital role as an effective “Higgsing” mechanism. We report a thorough numerical investigation of the confinement dynamics in SU(2) Yang-Mills theory by constructing such a statistical ensemble of correlated instanton-dyons.

---

## 1. Introduction

The Quantum Chromodynamics, or QCD, is established as the fundamental quantum field theory of strong nuclear force underlying all of nuclear physics. Despite its great success in describing an impressive variety of nuclear phenomena in Nature, a key aspect of QCD remains mysterious and poses a great challenge to our understanding. While the theory has quarks and gluons as its basic degrees of freedom in the Lagrangian, the colored quarks and gluons are absent from the observed physical spectrum in which the various color-singlet hadronic states emerge instead. This phenomenon, often referred to with the broad term “confinement” (see recent review in e.g. [1]), occurs also in a wide variety of QCD-like theories and notably in pure Yang-Mills theories. The latter fact makes it obvious that confinement arises from the nonperturbative gauge dynamics in the gluonic sector. It was suggested long ago [2–4], based on analogy with superconductivity, that the confinement may arise from chromo-magnetically charged gauge configurations with nontrivial topology with the vacuum being a “dual superconductor” of such magnetic objects (see review in e.g. [5]). This scenario is highly appealing and widely perceived to be a likely explanation. The idea was extensively explored via lattice simulations as well as has been concretely shown to work in certain supersymmetric theories. More

recently, the idea of “dual superconductor” vacuum has been further advanced into a “magnetic scenario” for the hot plasma phase in the temperature regime above but near the transition temperature  $T_c$  [6]: indeed if there is a magnetic superconductor below  $T_c$ , there should be a “precursor” i.e. the normal phase of thermal magnetic plasma just above  $T_c$ . There are strong evidences from lattice simulations [7–9] for this scenario and most interestingly such a magnetic component is found to be crucial for explaining a number of key transport properties of the QCD plasma near- $T_c$  as measured from heavy ion collision experiments [10–12]. Despite the various progress so far along this line of thought, it is nevertheless still unclear what types of configurations could drive confinement and how, in pure Yang-Mills and QCD-like (non-supersymmetric) theories.

Let us elaborate a bit on the difficulty to identify the relevant topological configurations for these theories. Conventional instantons (as well as their finite-temperature counterpart, the calorons) [13, 14] are well known topological objects and studied in details (see reviews in e.g. [15, 16]). However these conventional instantons/calorons only have *trivial holonomy*, that is, trivial Polyakov loop at spatial infinity  $|\vec{x}| \rightarrow \infty$  (— see Appendices A and B for a detailed discussion about holonomy), which is in sharp contrast to the confining vacuum where the holonomy is maximally nontrivial. Furthermore they are color neutral with no chromo-magnetic charge. Therefore such conventional instantons/calorons can not be responsible for confinement. Another natural candidate would be ’t Hooft-Polyakov type of magnetic monopole. However, a crucial difference of pure Yang-Mills or QCD (as compared with e.g. George-Glashow model or Seiberg-Witten theory) is that they do *not* have adjoint scalar fields which would provide the natural “Higgsing” on the spatial boundary, thus allowing the construction of magnetic monopole solutions. Because of this difficulty, one has to rely upon certain gauge-fixing procedure to manifest the monopoles in the pure Yang-Mills or QCD cases.

As it turns out, both difficulties are resolved recently in a crucial new development: the construction of *caloron solutions with nontrivial holonomy and nontrivial topology* to the classical Yang-Mills equations, known as the KvBLL calorons [17–19] (— see Appendix C for a detailed discussion). First of all, such new calorons by construction acquire the necessary sensitivity to holonomy and thus are able to play a role in the confinement dynamics. Even more nontrivially, such a caloron contains  $N_c$  different *dyons* (for  $SU(N_c)$  theory) which are chromo-magnetically charged and whose properties depend upon the holonomy. In these solutions, the nontrivial holonomy provides the needed nontrivial boundary constraints (that in “Higgsed” theories would come from the adjoint scalar fields). Owing to such important new features, the KvBLL calorons with their dyon constituents provide the unique topological configurations that could potentially account for the nonperturbative dynamics underlying confinement.

Based on the KvBLL solutions, a promising approach has emerged for understanding confinement in a statistical ensembles of dyons/anti-dyons from the constituents of the KvBLL calorons. Early works on an uncorrelated ensemble of these objects — to be called *instanton-dyons* (following recent literature) from now on in the present paper — already indicated that their contributions

(alone) to the holonomy potential tends to push the system toward confining holonomy [20–22]. However it was later found that such contributions would not be enough to overcome the one-loop perturbative contributions to the holonomy potential (which favors the trivial holonomy — see detailed discussions in Appendix B). It was later found by Shuryak and collaborators [23–27] that an effective dyon-anti-dyon interaction with a short-range repulsive core (or in a broader term, a strong dyon-anti-dyon short-range correlation) appears necessary to enforce the confining holonomy at temperatures lower than the confinement transition temperature  $T_c$ . Effective model for a Coulomb plasma of such dyons/antidions was also constructed and shown to give a reasonable description of the low temperature  $T < T_c$  properties of Yang-Mills theories [28, 29].

In this paper, we report a thorough numerical investigation of the confinement dynamics in SU(2) Yang-Mills theory by constructing such a statistical ensemble of correlated instanton-dyons. We present high precision results for the temperature dependence of the holonomy potential, the order parameter for confinement transition, the dyon ensemble properties (densities and density-density correlations), as well as the temporal and spatial Wilson loops. In particular we study the influence of the finite volume effect, the dyon-anti-dyon correlations as well as the screening mass on the confinement dynamics. Some of these results are considerably improved as compared with previous studies and many new results have not been previously reported.

The rest of the paper is organized as follows. In Section 2, we present the details for our construction of the correlated instanton-dyon ensemble and the numerical procedures. Our main results about the confinement dynamics in such an ensemble are reported in Section 3. The Section 4 then focuses on examining the consequences of the key parameters in the ensemble construction. Finally we conclude the study in Section 5. In addition a few Appendices are included to explain some “background” information in details and to make the paper more self-contained for the convenience of readers.

## 2. Construction of Correlated Instanton-Dyon Ensemble

### 2.1. The Partition Function

The construction of the partition function of the dyon ensemble begins with rewriting the one-loop quantum weight of the KvBLL caloron in the limit of large dyon separation Eq. (D.10) (refer to Appendices C and D for more details), namely the contribution of a pair of  $L$  and  $M$  dyons, in the following way

$$\mathcal{Z} = e^{-VP(\nu)} \int (d^3r_L f_L) (d^3r_M f_M) T^6 \det(\hat{G}). \quad (1)$$

Here, the fugacities per dyon species are introduced as  $f_M = \Gamma S^2 e^{-\nu S} \nu^{\frac{8\nu}{3}-1}$  and  $f_L = \Gamma S^2 e^{-\bar{\nu} S} \bar{\nu}^{\frac{8\bar{\nu}}{3}-1}$ . Extending this result to arbitrary number of  $L$  and  $M$  dyons requires to include the appropriate metric of the moduli space. As it was found in [20], it turns out the new metric can be approximated by the square of the determinant of a symmetric matrix  $G$  like  $\sqrt{\det(g)} \approx \det(G)$ ,

which in the  $SU(2)$  case when the number of  $L$  and  $M$  dyons are respectively  $N_L$  and  $N_M$ , the dimension of  $G$  is  $(N_L + N_M) \times (N_L + N_M)$  and its components are

$$G_{mi,nj} = \delta_{mn} \delta_{ij} \left( 4\pi\nu_m - \sum_{k \neq i} \frac{2}{T|\vec{r}_{m_i} - \vec{r}_{m_k}|} + \sum_k \frac{2}{T|\vec{r}_{m_i} - \vec{r}_{l_k}|} \Big|_{m \neq l} \right) + \frac{2\delta_{mn}}{T|\vec{r}_{m_i} - \vec{r}_{n_j}|} \Big|_{i \neq j} - \frac{2}{T|\vec{r}_{m_i} - \vec{r}_{n_j}|} \Big|_{m \neq n}, \quad (2)$$

where  $\vec{r}_{m_i}$  is the position vector of the  $i^{\text{th}}$  dyon of kind  $m$  (either  $L$  or  $M$ ). It is straightforward to see that for a single  $LM$  pair, the  $G$  matrix reduces to  $\hat{G}$  (Eq. (D.5)). Furthermore, it should be clear that these results are analogous for antidyons.

As it was pointed out in [21], dyon-antidyon configurations are not saddle points of the Yang-Mills action; however, the inclusion of anti-selfdual fields in the ensemble is done by factorizing the measure into uncorrelated parts  $\det(G_D) \det(G_{\bar{D}})$  ( $D$  for dyons and  $\bar{D}$  for antidyons) times a correlated contribution  $e^{-V_{D\bar{D}}}$ , where  $V_{D\bar{D}}$  is the action corresponding to dyon-antidyon interactions. Classical interactions between dyon-antidyon of the same kind was recently introduced in a gradient flow study in [25]. Using the parametrization found in [26], the potential takes the form

$$V_{L\bar{L}} = -2\bar{\nu}S \left( \frac{1}{\zeta_L} - 1.632e^{-0.704\zeta_L} \right), \\ V_{M\bar{M}} = -2\nu S \left( \frac{1}{\zeta_M} - 1.632e^{-0.704\zeta_M} \right), \quad \zeta_j = 2\pi\nu_j Tr_{j\bar{j}}. \quad (3)$$

for  $\zeta_j > \zeta_j^0 = 4$  and  $r_{j\bar{j}} = |\vec{r}_j - \vec{r}_{\bar{j}}|$ . Below the limit  $\zeta_j < \zeta_j^0$ , the interaction is repulsive and the proposed core potential for this region is given by

$$V_{j\bar{j}}^C = \frac{\nu_j V_c}{1 + e^{(\zeta_j - \zeta_j^0)}}, \quad (4)$$

where  $V_c$  is a constant that is tuned for the simulation.

Another interaction that has to be accounted for is the long-range forces due to the Abelian electric and magnetic charges and the nonlinear terms in the field strength tensor  $F_{\mu\nu}$ , given by

$$V_{ij} = \frac{S}{2\pi Tr_{ij}} (e_i e_j + m_i m_j - 2h_i h_j), \quad (5)$$

where  $e_j$  and  $m_j$  are the electric and magnetic charges (see Table C.1) and  $h_j = 1$  for the  $M$ -type (anti)dyons and  $-1$  for the  $L$ -type ones. As expected, this gives null classical interaction between the  $L$  and  $M$  dyons, namely the KvBLL

caloron. On the other hand, there is repulsive in the  $L\bar{M}$  and  $M\bar{L}$  channels, attractive for  $L\bar{L}$  and  $M\bar{M}$  and no interaction for the rest.

In the construction of the ensemble, one has to sum over different number of (anti)dyons, therefore some terms will not be neutrally charged such as in a Coulomb plasma. To account for the long range behavior of these interactions, one has regulate these terms by means of a screening Debye mass  $M_D$ . Thus, all Coulomb terms appearing in the ensemble (including those in the  $G$  matrices) are rewritten as  $\frac{1}{r} \rightarrow \frac{e^{-M_D r}}{r}$ .

Combining Eqs. (3) to (5), the action contribution to the uncorrelated part of the partition function is found to be

$$V_{D\bar{D}} = \begin{cases} \sum_{j>\bar{j}} 2S \left( \frac{1}{\zeta_j} - 1.632 e^{-0.704\zeta_j} \right) e^{-M_D r_{j\bar{j}}} & \text{if } \zeta_j > \zeta_j^0, \text{ for } L\bar{L}, M\bar{M} \\ \sum_{i>j} V_{ij}^C & \text{if } \zeta_j < \zeta_j^0, \text{ for } \begin{matrix} LL, \bar{L}\bar{L}, MM, \\ \bar{M}\bar{M}, L\bar{L}, M\bar{M} \end{matrix} \\ \sum_{i,\bar{j}} \frac{S}{\pi T r_{i\bar{j}}} e^{-M_D r_{i\bar{j}}} & \text{for } \bar{M}L, \bar{L}M \\ 0 & \text{for } LM, \bar{L}\bar{M}. \end{cases} \quad (6)$$

Now that the measure has been defined, the full partition function of the dyon-antidyon ensemble takes the form

$$\begin{aligned} \mathcal{Z} = e^{-VP(\nu)} & \sum_{\substack{N_M, N_L, \\ N_{\bar{L}}, N_{\bar{M}}}} \frac{1}{N_L! N_M! N_{\bar{L}}! N_{\bar{M}}!} \int \prod_{l=1}^{N_L} f_L T^3 d^3 r_{L_l} \prod_{m=1}^{N_M} f_M T^3 d^3 r_{M_m} \\ & \times \prod_{\bar{l}=1}^{N_{\bar{L}}} f_{\bar{L}} T^3 d^3 r_{\bar{L}_{\bar{l}}} \prod_{\bar{m}=1}^{N_{\bar{M}}} f_{\bar{M}} T^3 d^3 r_{\bar{M}_{\bar{m}}} \det(G_D) \det(G_{\bar{D}}) e^{-V_{D\bar{D}}}, \end{aligned} \quad (7)$$

where the factorial terms are introduced to avoid over counting of configurations.

This expression can be further simplified under the assumption of equal number of dyons and antidions of the same kind, reducing Eq. (7) to

$$\mathcal{Z} = e^{-VP(\nu)} \sum_{N_L, N_M} \left[ \frac{(f_L V T^3)^{N_L}}{N_L!} \frac{(f_M V T^3)^{N_M}}{N_M!} \right]^2 e^{-VT^3 \mathcal{F}(T, \nu)}, \quad (8)$$

where  $V$  is the 3D volume available and

$$e^{-VT^3 \mathcal{F}(T, \nu)} \equiv \int \prod_{l, m, \bar{l}, \bar{m}}^{N_L, N_M} \frac{d^3 r_{L_l} d^3 r_{M_m} d^3 r_{\bar{L}_{\bar{l}}} d^3 r_{\bar{M}_{\bar{m}}}}{V} \times \exp \{ \log [\det(G_D) \det(G_{\bar{D}})] - V_{D\bar{D}} \} \quad (9)$$

is the integral of all the space dependent factors. Finally, using Stirling's approximation  $\log N! \approx N \log N - N + \log \sqrt{2\pi N}$  and defining the dimensionless dyon densities as  $n_D = \frac{N_D}{VT^3}$ , we rewrite  $\mathcal{Z}$  as a sum of weights running over number of dyons as

$$\mathcal{Z} = \sum_{N_L, N_M} \exp \left[ -VT^3 \left( \frac{4\pi^2}{3} \nu \bar{\nu} + 2n_L \log \left( \frac{n_L}{f_L} \right) + 2n_M \log \left( \frac{n_M}{f_M} \right) + 2(n_L + n_M) + \frac{\log(4\pi^2 N_L N_M)}{VT^3} + \mathcal{F}(T, \nu) \right) \right] \quad (10)$$

$$\equiv \sum_{N_L, N_M} \mathcal{Z}_{LM}. \quad (11)$$

## 2.2. The Monte-Carlo Simulations

As opposed to how it was done in [24, 26, 27], in our simulation we used a flat geometry, namely a box with periodic boundary conditions. We believe this gives a more “realistic” approach to the model and a more direct way to compare the results with such as lattice simulations which are also done on a  $\mathbb{R}^3$  geometry.

From Eq. (11), it can be seen that all explicit dependence on the temperature  $T$  can be absorbed by rescaling  $rT \rightarrow r$ ,  $VT^3 \rightarrow V$ ,  $M_D/T \rightarrow M_D$  and the free energy  $F/T \equiv -\log \mathcal{Z} \rightarrow F$ . Since this simplifies the calculations, all the simulations are done using the latter scaled variables. However, the temperature dependence is then defined through the running of the coupling constant in the caloron action  $S$ , which at first loop approximation, is given by (see Appendix D)

$$S(T) = \frac{8\pi^2}{g^2(T)} = \frac{22}{3} \log \left( \frac{T}{\Lambda} \right), \quad (12)$$

where  $\Lambda$  is the scale parameter in the regularization. Therefore, by varying  $S$  as a parameter in the simulation, one can define  $\Lambda$  at the observed critical point ( $T = T_c$ ) and then establish the temperature dependence of the observables as  $T/T_c$ .

The computation of all the observables are performed through Monte Carlo simulations using the well known Metropolis-Hastings algorithm. Each configuration is generated by varying the 3D positions of a single (anti)dyon of each kind (accounting for the periodic boundary conditions), then apply the acceptance algorithm and in case of being accepted, move to the next set of dyons

and repeat the procedure. Once all positions have been accepted, we then move to compute the observables with that configuration and repeat all over again until the ensemble has been thermalized and we have significant statistics. It was found that after 1000 Monte Carlo configurations, the system was stabilized and the ensemble averages were calculated with 1500 subsequent configurations, for a total of 2500.

When it comes to compute the measure factors  $\det(G)$ , one has to notice that since it is an approximation to the actual moduli space metric, it may happen that some of the eigenvalues of the  $G$  matrices be negative thus violating the positive definiteness of the metric. This issue has been addressed in detail by [21, 28, 30]. To avoid configurations with negative eigenvalues in the simulations, the approach taken was using the Metropolis-Hastings algorithm to reject the configuration by assigning them a small statistical weight, i.e. if either  $G_D$  or  $G_{\bar{D}}$  has at least one negative eigenvalue, then the weight  $\exp(\log \det(G))$  is substituted by  $e^{-100}$ , which was found to be enough to create sufficient configurations with all positive eigenvalues.

One of the most important quantities calculated was the holonomy potential or free energy density. Due to the way its defined, the calculation through Monte Carlo is somehow tricky; however, there is a common way to do this computation. The only relevant term for the Monte Carlo simulation is  $e^{-V\mathcal{F}}$  since the other terms do not have spatial dependence. Therefore, the calculation can be done by introducing an auxiliary parameter  $\lambda$  as

$$e^{-V\mathcal{F}_\lambda(\lambda)} = \frac{\int \mathcal{D}r e^{-\lambda S_r}}{V^{2(N_L+N_M)}}, \quad S_r \equiv V_{D\bar{D}} - \log [\det(G_D) \det(G_{\bar{D}})], \quad (13)$$

where  $\mathcal{D}r$  is just the integration measure over all (anti)dyons positions. Then, through the standard Monte Carlo procedure, compute the ensemble average

$$\langle S_r \rangle (\lambda) \equiv \frac{\int \mathcal{D}r S_r e^{-\lambda S_r}}{\int \mathcal{D}r e^{-\lambda S_r}} = V \frac{\partial \mathcal{F}_\lambda}{\partial \lambda} \quad (14)$$

and finally integrate out the  $\lambda$  dependence to obtain the free energy contribution

$$\mathcal{F} = \frac{1}{V} \int_0^1 d\lambda \langle S_r \rangle (\lambda) = \mathcal{F}_\lambda(1), \quad (15)$$

given that  $\mathcal{F}_\lambda(0) = 0$ .

The volume of the box used on the first set of results was  $V = 43.37$  with a number of (anti)dyons of each kind running from  $N_D = 0$  to 22, i.e. the dyon density range spanned was  $n_D = 0$  to 0.5. In Section 4.1, we show some results with larger volumes, to explore finite volume effects in the observables. The model has three parameters which are fixed through all the temperature range covered, these are the Debye mass  $M_D$ , the core potential strength  $V_c$  and size  $\zeta_j^0$ . Although for the main results shown in the subsequent sections the values

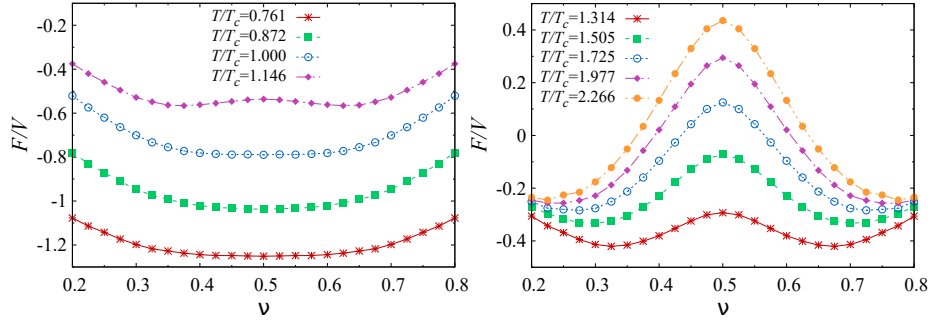


Figure 1: Free energy density of the dyon ensemble in the density range  $0 \leq n_D \leq 0.5$ .

used where 2, 20 and 2, respectively, in Sections 4.2 and 4.3 we show some results with different values.

### 3. Confinement-Deconfinement Transition

#### 3.1. The Holonomy Potential

One of the main quantities of interest in the study of thermodynamic properties and in particular for critical phenomena is the free energy density  $F = -\log \mathcal{Z}$ . Above some critical temperature  $T_c$ ,  $SU(2)$  pure gauge theory is expected to have a second order deconfinement phase transition, where the order parameter characterizing its criticality is the expectation value of the Polyakov loop at spatial infinity  $L_\infty$  (see Appendix B). When the gauge field is that of the KvBLL caloron, the order parameter takes the form  $\langle L_\infty \rangle = \cos(\pi\nu)$ , so one expects to observe the breaking of the  $Z_2$  symmetry of the theory through the free energy density, either as a function of  $L_\infty$  or  $\nu$ .

As it was mentioned earlier, the temperature dependence of all the observables in the ensemble was modulated by the instanton action  $S$  (Eq. (12)) which functioned as an input parameter in the simulation. Fig. 1 shows the free energy density for  $S = 5, 6, \dots, 13$ . It was found that for  $S = 5 - 7$  the minimum of the free energy density lies at  $\nu_{\min} = 0.5$ , namely maximal non-trivial holonomy. For  $S > 7$  the shape of  $F/V$  becomes that of a symmetric double well potential with  $\nu_{\min} < 0.5$ . It is important to mention that as expected for an  $SU(2)$  pure gauge theory,  $F/V$  is symmetric under the interchange  $\nu \rightarrow \bar{\nu}$ , therefore even though this was verified explicitly in the numerical calculations, data points in the domain  $(0.5, 0.8]$  of all free energy density plots are just reflections of the actual simulation results done for  $\nu \in [0.2, 0.5]$ .

To verify with greater accuracy that  $S = 7$  corresponds to the critical temperature, we ran the simulation for  $S = 7.25, 7.5$  and  $7.75$ . As it is shown on Fig. 2, for  $S \geq 7.25$  the  $Z_2$  symmetry is broken and the minimum of the free energy density is  $\nu_{\min} \neq 0.5$ . Thus, at this precision, we define the critical temperature at  $S = 7$ , which lets us fix our scale parameter from Eq. (12) at



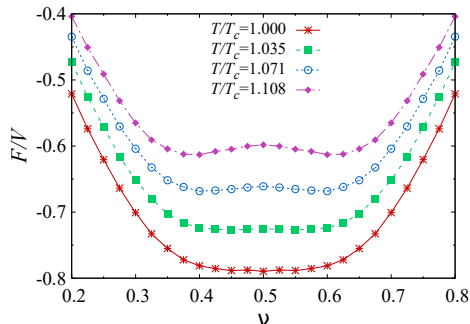


Figure 2: Free energy density of the dyon ensemble near  $T_c$  ( $S = 7$ ) in the density range  $0 \leq n_D \leq 0.5$ .

$\Lambda = 0.385T_c$  and express all temperature dependent quantities in terms of the ratio  $T/T_c$ .

The expectation value  $\langle L_\infty \rangle$ , was found by fitting the free energy density near the minima to a quadratic function with 5 points and then, through a derivative test on the fit, find its minimum. This fit was used as well to obtain the Debye screening mass  $M_D$  as will be shown in Section 4.3.

An insightful check of the role of  $L_\infty$  as an order parameter of the deconfinement phase transition is through universality considerations. The well known Svetitsky-Yaffe conjecture [31], relates  $SU(2)$  pure gauge theory in  $(3+1)$  dimensions to the  $3D$  Ising model of ferromagnetism by categorizing both in the same universality class, which has been proven several times in different numerical studies such as [32–37]. In this sense,  $L_\infty$  becomes the analog of the magnetization, thus its critical behavior must follow the power law

$$\langle L_\infty \rangle = a(T/T_c - 1)^\beta [1 + b(T/T_c - 1)^\omega]. \quad (16)$$

Using the well established values of the critical exponents of the  $3D$  Ising model  $\beta \approx 0.3265$  and  $\omega \approx 0.84$  [38], on Fig. 3 we show the fitted curve obtained from the numerical results of the dyon ensemble near  $T_c$ , namely  $1 \leq T/T_c \leq 1.505$ . This result shows the continuous nature of the phase transition and is in qualitative agreement with the lattice results from [39].

As for the expectation value of dyon densities, depicted in Fig. 4, one can see that at  $T \leq T_c$ , the  $L$  and  $M$  type densities are fairly equal. In the confined phase, the preferred holonomy corresponds to the maximal non-trivial one where both dyon types have the same core radius and therefore equal weight in the partition function. For  $T > T_c$ , the preferred holonomy starts to shift towards the trivial one ( $\nu \rightarrow 0$ ) and the  $M$  dyons become larger and larger. Recalling from the KvBLL caloron solution (see Appendix C), in the limit of trivial holonomy, the  $L$  dyon disappears and the field becomes that of the Harrington-Shepard caloron. A similar situation is observed in the ensemble, as temperature is increased, the  $L$  dyon density decreases much faster than  $M$  one to the point where it is close to zero.

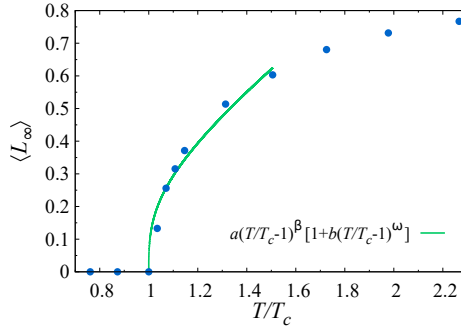


Figure 3:  $L_\infty$  as an order parameter of the phase transition.

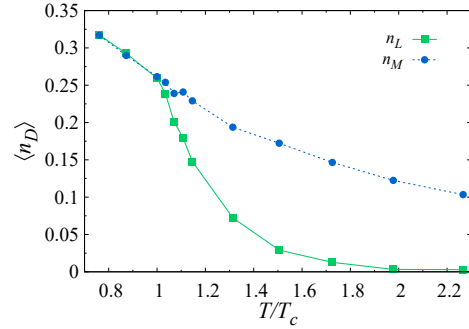


Figure 4: Temperature dependence of the ensemble average of dyon densities.

### 3.2. The Dyon and Antidyon Spatial Correlations

The 2-particle space dependent correlations, namely

$$G_{DD'}(|\vec{x}|) = \frac{\frac{1}{V} \left\langle \sum_{i=1}^{N_D} \sum_{j=1}^{N_{D'}} \Theta_{\delta x}(r_{ij} - |\vec{x}|) \right\rangle}{n_D n_{D'} \frac{4\pi}{3} [(|\vec{x}| + \delta x)^3 - |\vec{x}|^3]}, \quad (17)$$

which is normalized to that of an uncorrelated ideal gas and where the step function  $\Theta_{\delta x}(\xi) = 1$  for  $0 < \xi < \delta x$  and 0 otherwise, are shown on Figs. 5 to 9 for all different (anti)dyon pairs combinations. Each one of the correlations are depicted for both confined and deconfined phases for which the holonomy parameter  $\nu$  was fixed according to the one which minimized the action at the corresponding temperature. In addition, the number of dyons  $N_D$  of each correlator was fixed to the (density) ensemble average discussed in the previous section (Fig. 4).

The presence of the core potential is clearly observed for all the dyon pairs, besides the  $LM$  for which there is none. At distances right above the core size  $\zeta_j^0/2\pi\nu_j$  the correlation functions seem to have a small bump that rapidly goes to one indicating there is no more correlation at large separations and that the main contribution to the dyon interactions comes indeed from the core.

### 3.3. The Polyakov Loop Correlator

In the large distance limit ( $|\vec{x}| \rightarrow \infty$ ), the  $A_4$  component of the dyon fields becomes Abelian (see Appendix C). However, the total  $A_4$  of the ensemble (far away from their individual cores) cannot be given by a superposition of the individual fields of all dyons yet. Since the asymptotic condition  $A_4|_{|\vec{x}| \rightarrow \infty} = \pi\nu\tau^3$  must be satisfied, one has to eliminate the holonomy parameter term in the field by means of the time dependent gauge transformation  $U = \exp(-i\pi\nu x_4 \tau^3)$ ,

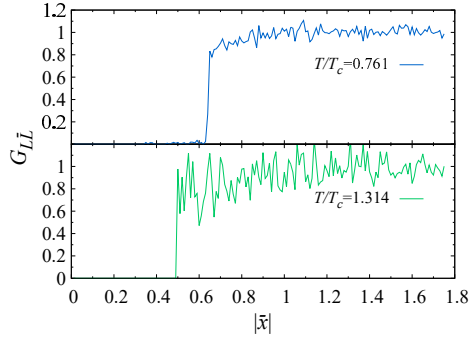


Figure 5: 2-particle spatial correlations for  $LL$  dyon pairs at the confined and deconfined phases.

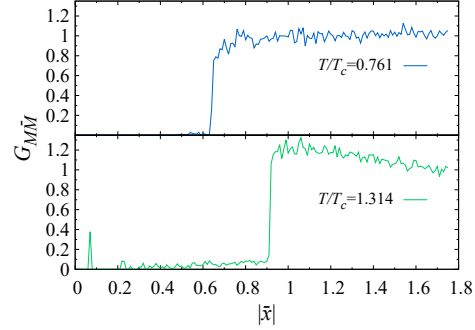


Figure 6: 2-particle spatial correlations for  $MM$  dyon pairs at the confined and deconfined phases.

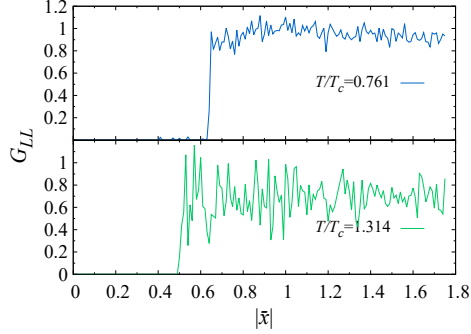


Figure 7: 2-particle spatial correlations for  $LL$  dyon pairs at the confined and deconfined phases.

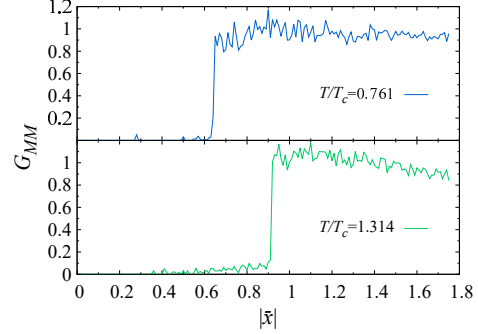


Figure 8: 2-particle spatial correlations for  $MM$  dyon pairs at the confined and deconfined phases.

then superimpose all dyonic fields and finally restore the asymptotic term with the inverse gauge transformation  $U^\dagger$  [25], leading to

$$A_4(\vec{x}) = \frac{\tau^3}{2} [2\pi\nu + l(\vec{x})], \quad (18)$$

where  $l(\vec{x})$  is the sum of all Coulomb terms of dyons and antidyons

$$l(\vec{x}) \equiv \sum_{l,m}^{N_L, N_M} \left( \frac{1}{|\vec{x} - \vec{r}_{L_l}|} - \frac{1}{|\vec{x} - \vec{r}_{M_m}|} + \frac{1}{|\vec{x} - \vec{r}_{\bar{L}_l}|} - \frac{1}{|\vec{x} - \vec{r}_{\bar{M}_m}|} \right). \quad (19)$$

In the study of confinement, it is of most importance to look at the interaction between a static (infinitely heavy) quark-antiquark pair. A successful confining theory should have an asymptotically linear rising potential at large separations between the static sources. At finite temperature, the color averaged heavy quark-antiquark free energy  $F_{q\bar{q}}^{\text{avg}}$  is defined through the expectation

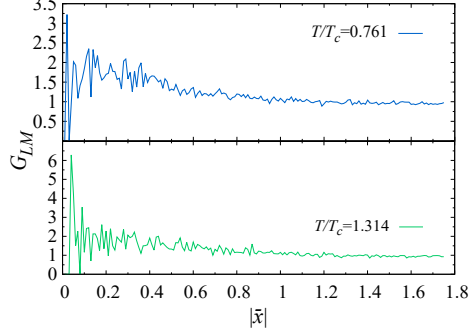


Figure 9: 2-particle spatial correlations for  $LM$  dyon pairs at the confined and deconfined phases.

value of traced Polyakov loop correlators (see Appendix B). For quarks in the fundamental representation, from Eqs. (18) and (19) and the definition of the Polyakov loop, it is straightforward to see that

$$\frac{1}{2} \text{Tr} L^f(\vec{x}) = \cos \left[ \pi\nu + \frac{1}{2} l(\vec{x}) \right], \quad (20)$$

thus defining the color averaged static quark-antiquark potential in the dyon ensemble as

$$e^{-F_{q\bar{q}}^{\text{avg}}} \equiv \frac{1}{4} \langle \text{Tr} L^{\dagger f}(\vec{x}) \text{Tr} L^f(\vec{y}) \rangle = \left\langle \cos \left[ \pi\nu + \frac{1}{2} l(\vec{x}) \right] \cos \left[ \pi\nu + \frac{1}{2} l(\vec{y}) \right] \right\rangle. \quad (21)$$

Moreover, according to the color decomposition  $3 \otimes \bar{3} = 1 \oplus 3$ , an  $SU(2)$  quark-antiquark pair can interact through a singlet and a triplet channel [40], meaning that  $F_{q\bar{q}}^{\text{avg}}$  is decomposed into

$$e^{F_{q\bar{q}}^{\text{avg}}} = \frac{1}{4} e^{-F_{q\bar{q}}^1} + \frac{3}{4} e^{-F_{q\bar{q}}^3}, \quad (22)$$

where the singlet free energy is given by

$$e^{-F_{q\bar{q}}^1} \equiv \frac{1}{2} \langle \text{Tr} [L^{\dagger f}(\vec{x}) L^f(\vec{y})] \rangle = \left\langle \cos \left[ \frac{l(\vec{x}) - l(\vec{y})}{2} \right] \right\rangle \quad (23)$$

and the triplet contribution follows trivially from Eq. (22).

On Fig. 10 we show the singlet channel free energy as a function of interquark separation  $|\vec{x} - \vec{y}|$  for temperatures below and above  $T_c$ . Due to the periodic boundary conditions imposed in our geometry, the maximum allowed distance is  $|\vec{x} - \vec{y}| \leq R/2$ , where  $R \approx 3.51$  is the size of the box of volume  $V = 43.37$ . To compute these observables, we generated 2500 Monte Carlo configurations for each combination of number of dyons ( $N_L, N_M = 0, \dots, 22$ ). To account for isotropy, for each interquark separation we averaged the contribution to the Polyakov loop correlator from 13 different orientations.

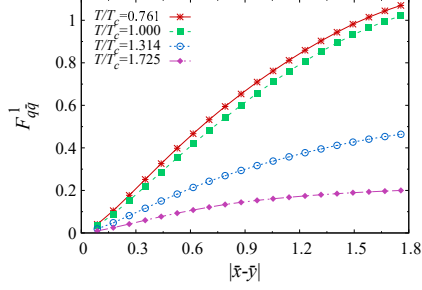


Figure 10: Singlet channel of the static quark-antiquark potential in the fundamental representation at confined and deconfined phases for  $\nu = 0.5, 0.5, 0.35$  and  $0.275$ , in order of increasing temperature.

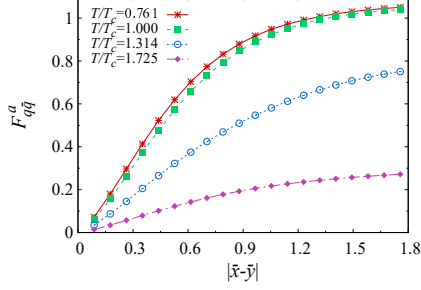


Figure 11: The static quark-antiquark potential in the adjoint representation at the confined and deconfined phases for  $\nu = 0.5, 0.5, 0.35$  and  $0.275$ , in order of increasing temperature.

For each temperature, the holonomy parameter  $\nu$  was fixed to the one which minimized the ensemble free energy  $F = -\log \mathcal{Z}$ , namely the one with the highest statistical weight in the ensemble. On Figs. 12 and 13, we show the color averaged potential and its singlet and triplet contributions for the confined and deconfined phases at  $T/T_c = 0.761$  and  $T/T_c = 1.725$ .

For the case of adjoint static quarks, the Polyakov loop in the adjoint representation is needed. Following [41], we have that it can be obtained from the fundamental one  $L^f$  as

$$L_{ij}^a = \frac{1}{2} \text{Tr} (\tau_i L^f \tau_j L^{\dagger f}), \quad (24)$$

where  $\tau_i$  are the Pauli matrices. Given that  $L \in SU(2)$ , in the fundamental representation is generally defined as

$$L^f = a_0 \mathbb{1} + a_i \tau_i, \quad (25)$$

with  $a_\mu a_\mu = 1$ . Thus Eq. (24) can be rewritten as

$$L_{ij}^a = 2 \left[ a_0 a_k \varepsilon_{ijk} + a_i a_j + \delta_{ij} \left( a_0^2 - \frac{1}{2} \right) \right], \quad (26)$$

and it is easy to see that its trace is expressed in terms of the fundamental one as

$$\text{Tr} L^a(\vec{x}) = |\text{Tr} L^f(\vec{x})|^2 - 1. \quad (27)$$

The adjoint static quark-antiquark free energy is then defined as

$$e^{-F_{q\bar{q}}^a} = \frac{\langle \text{Tr} L^{\dagger a}(\vec{x}) \text{Tr} L^a(\vec{y}) \rangle}{\langle |\text{Tr} L^a(0)|^2 \rangle}. \quad (28)$$

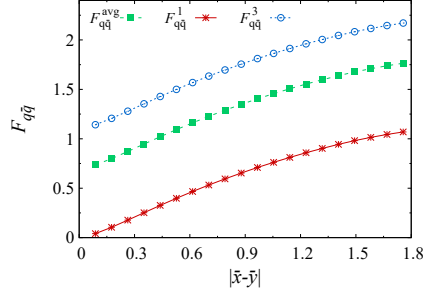


Figure 12: Color averaged with the singlet and triplet channels of the static quark-antiquark potential in the confined phase at  $T/T_c = 0.761$  and  $\nu = 0.5$ .

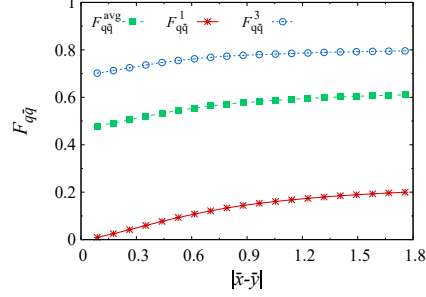


Figure 13: Color averaged with the singlet and triplet channels of the static quark-antiquark potential in the deconfined phase at  $T/T_c = 1.725$  and  $\nu = 0.275$ .

Notice we have included a normalization factor  $\langle |\text{Tr } L^a(0)|^2 \rangle$  in the correlator such that  $F_{q\bar{q}}^a = 0$  at  $|\vec{x} - \vec{y}| = 0$ . The resulting potentials are shown in Fig. 11 for different temperatures.

As it was mentioned earlier, at large separations in the confined region, one expects the static potential to have a linear rising of the form

$$F_{q\bar{q}}|_{|\vec{x}-\vec{y}|\rightarrow\infty} \approx \sigma|\vec{x} - \vec{y}|, \quad (29)$$

where  $\sigma$  is the so called *string tension*. This is clearly observed in the fundamental representation (Fig. 10) at  $T/T_c \leq 1$ . However, at temperatures above  $T_c$ , the slope  $\sigma$  starts to decrease until it reaches values close to zero, meaning that the deconfined phase has been reached. On Fig. 14, we show the extracted string tensions for the color averaged potential for several temperatures. The linear fits used, were done ignoring the “curved” tails observed at large distances, since we believe those are due to finite volume effects (See Section 4.1). Despite that in a true phase transition one expects a rapid decrease in  $\sigma$  right above  $T_c$ ; our results show a slower decrease, an effect which may be due to finite volume issues.

For the adjoint potential, the expected saturation at a certain distance was observed. This due to “string breaking” caused by the color screening of gluons in the adjoint representation.

In a nutshell, our results for the static quark-antiquark potentials in both representations reproduced the expected behaviour of an  $SU(2)$  pure gauge theory. Furthermore, are qualitatively in agreement with lattice results of caloron ensembles such as in [22].

### 3.4. The Spatial Wilson Loop

For quite some time, it has been argued that spatial Wilson loops at finite temperature do not provide a good measure of the deconfinement phase transition, given that even above  $T_c$  they show area law behavior and an increase

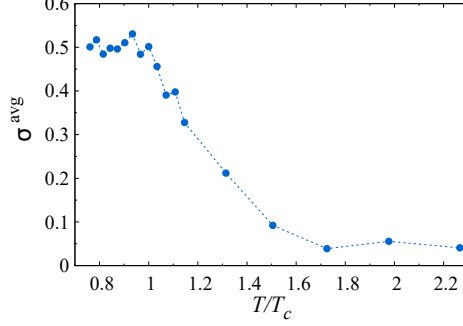


Figure 14: Temperature dependence of the dimensionless string tension  $\sigma^{\text{avg}}$  extracted from the color averaged static quark-antiquark potential  $F_{q\bar{q}}^{\text{avg}}$  in the fundamental representation.

of the spatial string tension  $\sigma_s$  [42–45]; nonetheless, the restoration of Lorentz symmetry (Euclidean  $O(4)$ ) at  $T \rightarrow 0$  suggests that in this limit,  $\sigma_s$  should coincide with the string tension of the static quark potential Eq. (29) extracted from Polyakov loop correlators.

The  $SU(2)$  traced spacial Wilson loop is defined as

$$W_C \equiv \frac{1}{2} \text{Tr} \mathcal{P} \exp \left[ i \oint_C dx_i A_i(x) \right] = \frac{1}{2} \text{Tr} \mathcal{P} \exp \left[ i \int_{A_C} da_i B_i(x) \right], \quad (30)$$

where  $B_i \equiv \frac{1}{2} \varepsilon_{ijk} F_{jk}$  is the magnetic field and  $A_C$  is the area enclosed by a rectangular contour  $C$ .

In the gauge where  $A_4(x)$  is diagonal (see Appendix C), the only non-vanishing spatial component of the dyon fields in the asymptotic limit is

$$A_\phi^j(\vec{x}) = m_j \frac{\tan \frac{\theta}{2} \tau^3}{r}, \quad (31)$$

where  $m_j = \pm 1$  is the corresponding magnetic charge (Table C.1) and  $r = \sqrt{x_i x_i}$ . The Dirac string singularity along the negative  $x_3$ -axis, although a gauge artifact, might be an inconvenience for the numerical simulations; therefore, for computing  $W_C$  it is more suitable to use the magnetic field

$$B_r^j = \frac{m_j \tau^3}{r^2}, \quad (32)$$

with  $B_\phi = B_\theta = 0$ . The total field of the ensemble of dyons will thus be

$$B_i(\vec{x}) = \frac{\tau^3}{2} \sum_{l,m}^{N_L, N_M} \left[ \frac{(\vec{x} - \vec{r}_{L_l})_i}{|\vec{x} - \vec{r}_{L_l}|^3} - \frac{(\vec{x} - \vec{r}_{M_m})_i}{|\vec{x} - \vec{r}_{M_m}|^3} - \frac{(\vec{x} - \vec{r}_{\bar{L}_l})_i}{|\vec{x} - \vec{r}_{\bar{L}_l}|^3} + \frac{(\vec{x} - \vec{r}_{\bar{M}_m})_i}{|\vec{x} - \vec{r}_{\bar{M}_m}|^3} \right]. \quad (33)$$

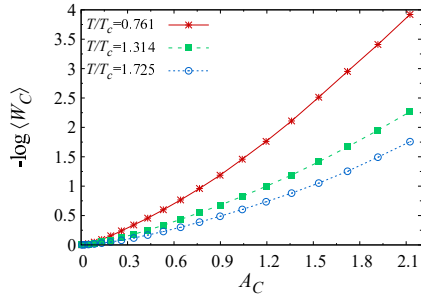


Figure 15: Area law for the spatial Wilson loop in the fundamental representation at confined and deconfined phases.

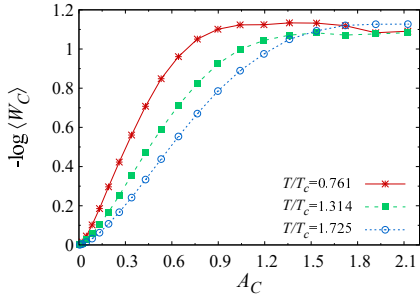


Figure 16: Area law of the spatial Wilson loop in the adjoint representation at confined and deconfined phases.

The interest is to show that the spatial Wilson loop in the dyon ensemble will follow the area law

$$\langle W_C \rangle \sim e^{-\sigma_s A_C} \quad (34)$$

in both confining and deconfined phases. On Fig. 15, the negative logarithm of  $\langle W_C \rangle$  in the fundamental representation is plotted as a function of  $A_C$  and it can be seen that for large contour areas, indeed has an almost linear rising.

Recalling the units used in this work, the string tension obtained here is dimensionless, meaning that restoring physical units it goes as  $\sigma_s \rightarrow \sigma_s/T^2$ . As has been established before,  $\sigma_s$  increases with  $T$ ; however,  $\sigma_s/T^2$  should decrease as the temperature rises [44], which is in fact in agreement with our results. Finally, for the adjoint representation, shown in Fig. 16, the “potential” reaches a plateau much faster than that of  $F_{q\bar{q}}^a$ , a stronger indication of the screening effects for adjoint sources.

## 4. Discussions

### 4.1. Finite volume effects

A rigorous study of all thermodynamic quantities implies an infinite volume limit. The constructed dyon ensemble clearly suffers of volume limitations, specifically when dealing in the lower temperature regimes where dyon densities are large. Larger volumes requires larger number of dyons and therefore more computing power. To look into the possible effects which finite volume have on the observables calculated, we performed tests increasing the volume of the box to two and three times the previous volume used, which for this section we will denote  $V_0 = 43.37$ .

As it was mentioned before, at the original volume used, the observables were computed using the full range of dyon densities rather than just fixing the maximum contribution of the partition function  $\mathcal{Z}$ . This was mainly because of two reasons. The first one has to do with precision, since the distribution  $\mathcal{Z}_{\text{LM}}/\mathcal{Z}$  as a function of dyon densities was not sharp enough, we wanted to include all



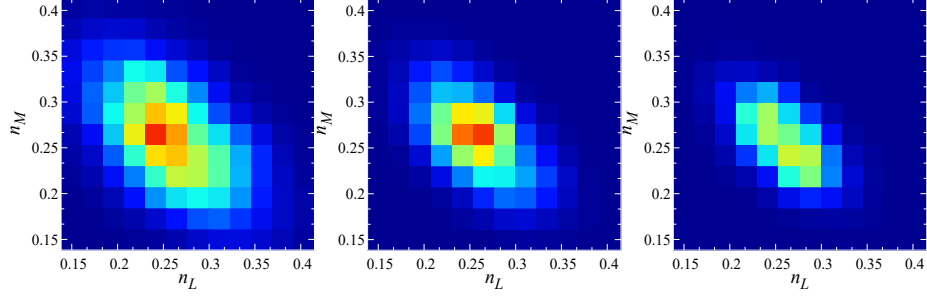


Figure 17: Dyon density dependence of  $Z_{LM}/Z$  for different volumes (from left to right:  $V_0$ ,  $2V_0$  and  $3V_0$ ) at the phase transition  $T/T_c = 1$  and  $\nu = 0.5$ .

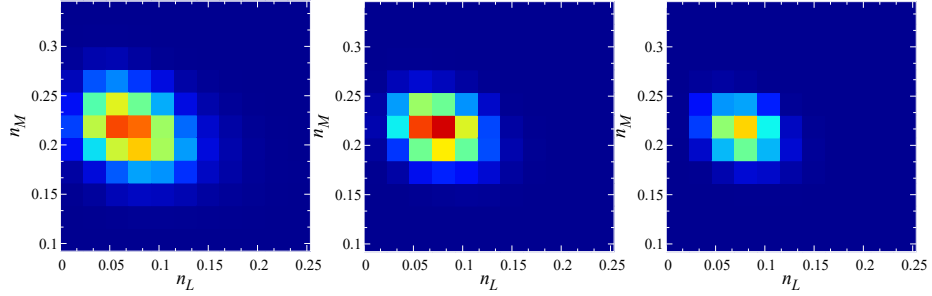


Figure 18: Dyon density dependence of  $Z_{LM}/Z$  for different volumes (from left to right:  $V_0$ ,  $2V_0$  and  $3V_0$ ) in the deconfined phase  $T/T_c = 1.314$  and  $\nu = 0.35$ .

possible contributions of different densities in the observables, leading to more reliable calculations. The second one was due to the fact that the maximum of the partition function shifted significantly with temperature and holonomy parameter  $\nu$ , thus one would have to choose different fixed densities for each combination of parameters in the simulation. We concluded that exploring a whole range of densities would be more suitable for this work.

On Figs. 17 and 18, we show how the partition function is changed as the volume is increased. As expected, the distribution becomes sharper and most importantly the location of the maximum does not change by much. Table 1 contains numerical values of ensemble averages of the dyon densities at different temperatures as well as the free energy density for  $\nu_{\min}$  obtained at  $V_0$ . It can be seen that the volume effects in the densities are significantly smaller than in the free energy density, which in fact are considerably small.

Another test on the influence of volume was done with the static quark-antiquark potentials. As mentioned in the previous section, the potentials exhibited a small curved tail near the largest distances as opposed to be completely linear. To test if this was a consequence of the finite volume, on Fig. 19 we show the results of the singlet channel potential calculated in a box twice the size of the previous volume used. For comparison, we also included the original potentials. One can see that indeed, the curved tails only appear at the edge of the

	$T/T_c$	$V_0$	$2V_0$	$3V_0$
$F/V$	0.761	-1.251	-1.275	-1.283
	1.000	-0.790	-0.813	-0.826
	1.314	-0.416	-0.433	-0.444
$\langle n_L \rangle$	0.761	0.317	0.320	0.315
	1.000	0.259	0.259	0.260
	1.314	0.075	0.077	0.077
$\langle n_M \rangle$	0.761	0.317	0.315	0.312
	1.000	0.261	0.262	0.259
	1.314	0.215	0.216	0.215

Table 1: Volume dependence of the free energy density and ensemble averages of dyon densities for  $V = V_0, 2V_0$  and  $3V_0$ , with  $V_0 = 43.37$ .

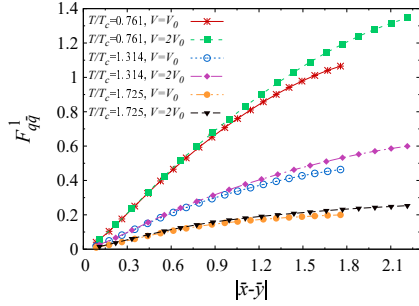


Figure 19: Volume effects on the singlet channel of the static quark-antiquark potential at confined and deconfined phases.

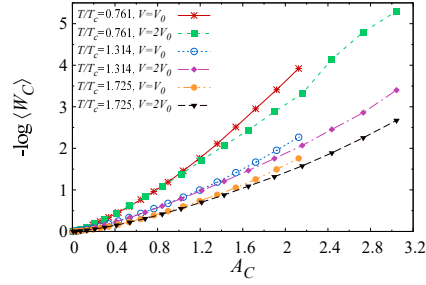


Figure 20: Volume effects on the area law of the spatial Wilson loop at confined and deconfined phases.

box and at intermediate distances both potentials match substantially well. The same behavior is observed for the spatial Wilson loop in Fig. 20, the “bending” of the curves near the largest values of  $A_C$  is smeared for  $V = 2V_0$ .

#### 4.2. The Influence of Dyon-Antidyon Short-Range Correlation

One of the most important parts for the confinement mechanism in this model is the introduction of the core potential  $V_{jj}^C$ . As it was shown on Eq. (4), there are two parameters which define the interaction:  $V_c$  is the strength and  $\zeta_j^c$  the size of the core. The value these parameters take have a strong influence in the observables calculated. On Figs. 21 to 23 we show the free energy density as a function of  $\nu$  for different values of  $V_c$  at different temperatures. We observed, that for  $V_c = 10$  the system was never found in the confined phase, meaning that  $\langle L_\infty \rangle \neq 0$  in the temperature range explored. On the opposite side, on Fig. 22 for  $V_c > 20$ , the curve around the minimum  $\nu_{\min} = 0.5$  is not as flat as for  $V_c = 20$ , suggesting that the critical temperature will be shifted and no longer correspond to  $S = 7$ . Recalling that  $T/T_c = 1$  is defined for a whole

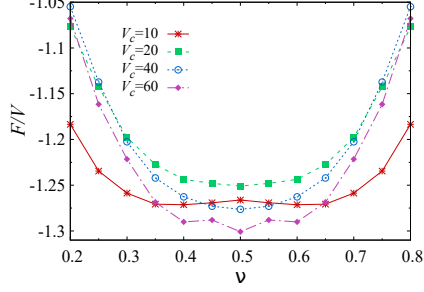


Figure 21: Effect of the core potential on the free energy density at  $T/T_c = 0.761$ .

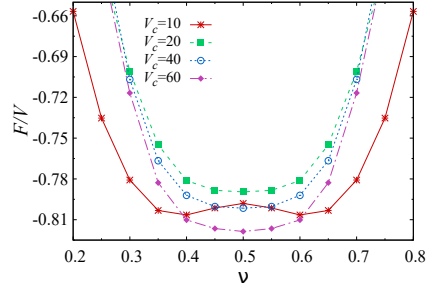


Figure 22: Effect of the core potential on the free energy density at  $T/T_c = 1.000$ .

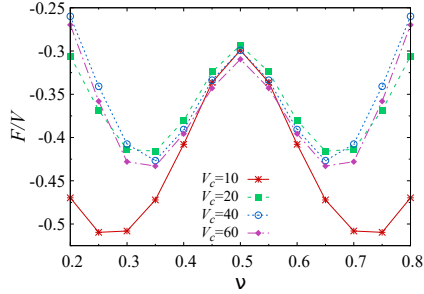


Figure 23: Effect of the core potential on the free energy density at  $T/T_c = 1.314$ .

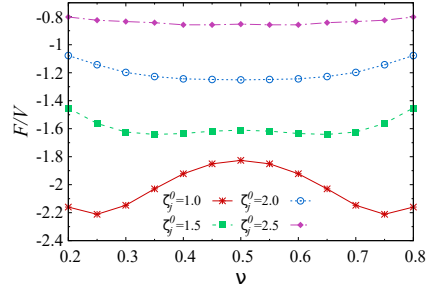


Figure 24: Effect of the core potential on the free energy density at  $T/T_c = 0.761$ .

set of parameters fixed, namely  $V_c = 20$ ,  $\zeta_j^0 = 2$ ,  $M_D = 2$  and  $V = 43.37$ , it is important to point out that a change in any of these will shift the location of the free energy minima and therefore the critical point, which is also essential to fix the scale parameter of the theory  $\Lambda$ .

In a similar fashion, a change in the core size  $\zeta_j^0$ , will also modify the shape of the free energy, although in a more drastic way. The dyon-antidyon interaction proposed in [25] is valid for  $\zeta_j^0 > 4$ ; however, in their subsequent works [26, 27] the parameter used was  $\zeta_j^c = 2$ , as it is for the first results shown in this article. Interested in the effects of the core size, we computed the  $\nu$  dependence of the free energy density for  $\zeta_j^0 = 1, 1.5$  and  $2.5$  (Figs. 24 to 26). The main reason why we could not use larger values, specially  $\zeta_j^0 = 4$ , was due to volume limitations since the latter case implies interdyon separations in the interval  $1.27 \leq r_{j\bar{j}} \leq 3.18$ ; however, for the volume used in this section ( $V = 43.37$ ), the largest available interdyon distance is  $r_{j\bar{j}} \approx 1.75$ , thus resulting in the unphysical situation where most of the configurations will always lie inside the core region.

As the core size is decreased, the holonomy starts approaching the trivial one favoring the deconfining phase even at the lowest temperature explored.

Even though, as we have seen in the previous section, there were not significant volume effects at  $V_c$  and  $\zeta_j^0$  fixed, it would be of interest to explore large

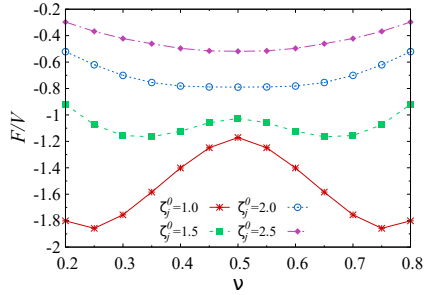


Figure 25: Effect of the core potential on the free energy density at  $T/T_c = 1.000$ .

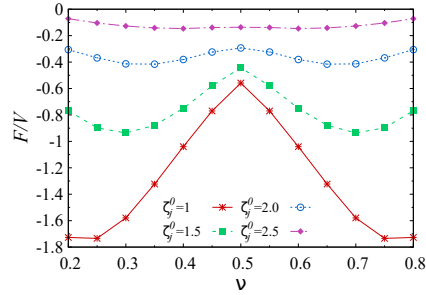


Figure 26: Effect of the core potential on the free energy density at  $T/T_c = 1.314$ .

volume ensembles with larger core sizes; however, a more efficient method of calculation would be necessary to reduce computing time.

#### 4.3. The Debye Screening Mass

The Debye mass  $M_D$  used to regularize the large distance behavior of the Coulomb terms and therefore to account for the screening of charge, is used in the ensemble as an input parameter. Nevertheless, the effective holonomy potential or free energy should contain information in the vicinity of its minimum value. The electric screening mass, which we will associate to  $M_D$ , is then given by the curvature of the free energy around its minimum, i.e.

$$M_D^2 = \frac{2S}{V} \left. \frac{\partial^2 F}{\partial \nu^2} \right|_{\nu_{\min}}. \quad (35)$$

To extract its value from the ensemble results, we made a quadratic fit using five points in the neighborhood of the free energy minima, namely the same fit used to calculate  $\nu_{\min}$  in Section 3.1. On Fig. 27, we show the results of this calculation as a function of temperature. As expected from a second order phase transition, at the critical temperature,  $M_D$  is close to zero since the free energy density is almost flat around the minimum  $\nu_{\min} = 0.5$ . For higher temperatures, it seems to be stabilized even though the values calculated oscillate between 1.6 and 2.0, approximately. It should be noticed that this calculation is dependent on the fit applied to the free energy density; however, our results are qualitatively in agreement with the lattice calculations in [39].

The effects of  $M_D$  as input parameter in the dyon ensemble are shown in Figs. 28 to 30, with the free energy density at different temperatures. Fixing all other parameters as in the first set of results, we chose  $M_D = 1.5$  and 3.0.

## 5. Conclusion

Confinement is a remarkable nonperturbative phenomenon in pure Yang-Mills and QCD-like theories. The mechanism of confinement remains a sig-

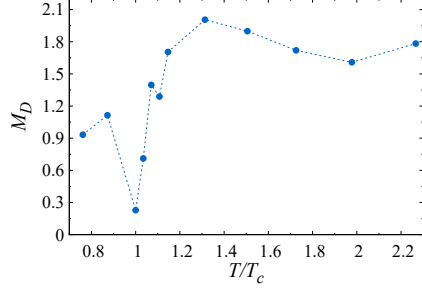


Figure 27: Debye mass obtained from  $M_D^2 = \frac{2S}{V} \left. \frac{\partial^2 F}{\partial \nu^2} \right|_{\nu_{\min}}$ , using  $M_D = 2$  as input parameter in the simulation.

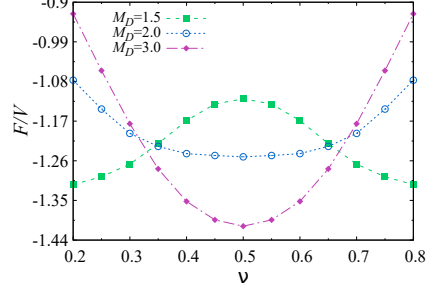


Figure 28: Free energy density for different values of the Debye screening mass  $M_D$  at  $T/T_c = 0.761$

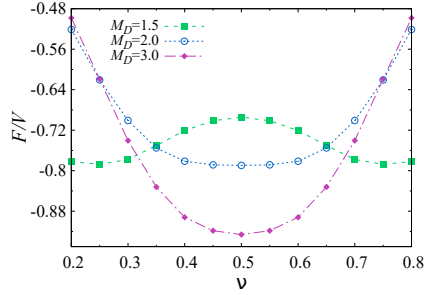


Figure 29: Free energy density for different values of the Debye screening mass  $M_D$  at  $T/T_c = 1.000$ .

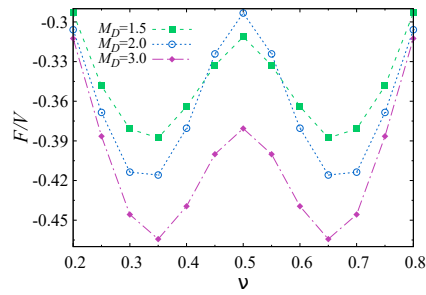


Figure 30: Free energy density for different values of the Debye screening mass  $M_D$  at  $T/T_c = 1.314$ .

nificant challenge to our understanding and is generally believed to pertain to certain nontrivial topological configurations of the gluonic sector. The recently found KvBLL caloron solutions with nontrivial holonomy, consisting of constituent dyons, have provided a concrete and promising path of investigation. In this paper, we have constructed a statistical ensemble of such correlated instanton-dyons and performed a thorough numerical study of its various properties for the  $SU(2)$  Yang-Mills theory. Our main conclusion is that such an ensemble correctly produces the various essential features of the confinement dynamics from above to below the transition temperature. These features include the evolution of holonomy potential with temperature, a second order phase transition in terms of the order parameter (Polyakov loop expectation value), the linear static quark-anti-quark potential, etc. We have also found that the confinement dynamics is very sensitive to both the implemented short-range dyon-anti-dyon correlations and the Debye screening effect in the many-body ensemble by quantifying how the holonomy potential changes with these parameters. Given such success, it appears reasonable to believe that the ensemble of correlated instanton-dyons may indeed hold the key of confinement mechanism. The natural next steps of investigation would be the extension of the present

work toward the  $SU(3)$  case as well as toward the inclusion of dynamic fermions thus allowing the study of nontrivial interplay between the confinement transition and the spontaneous chiral symmetry breaking, which we shall report elsewhere in the future.

## Acknowledgements

The authors are particularly grateful to E. Shuryak for many helpful discussions. The authors also thank R. Larsen, R. Pisarski, I. Zahed, and A. Zhitnitsky for useful discussions and communications. This work is supported by the National Science Foundation under Grant No. PHY-1352368. MALR is in addition supported by CONACyT under Doctoral supports Grants No. 669645. The computation of this research was performed on IU's Big Red II cluster that is supported in part by Lilly Endowment, Inc. (through its support for the Indiana University Pervasive Technology Institute) and in part by the Indiana METACyt Initiative.

## A. Holonomy, Polyakov Loop, and Center Symmetry

The classification of fiber bundles is an interesting topic in the geometry. Holonomy group, which describes the vector parallel transportation around closed loops, is one of tools to characterize the connection structure of a bundle. In gauge field theory the Wilson loop plays the same role as holonomy for gauge connections

$$W[A_\mu] = \mathcal{P} \exp \left( i \oint dx^\mu A_\mu(x) \right) \quad (\text{A.1})$$

In the imaginary-time formalism of finite temperature field theory the temporal direction is compactified to a circle of radius  $(2\pi T)^{-1}$ , where  $T$  is the temperature. Therefore the holonomy could be defined around this loop as

$$L[A_\mu] = \mathcal{P} \exp \left( i \int_0^{1/T} dx_4 A_4(\vec{x}, x_4) \right) \quad (\text{A.2})$$

which is the so-called Polyakov loop. Here  $A_4$  is an element of Lie algebra  $\mathfrak{su}(N)$ . And it could have different forms in different representations. Practically the Polyakov loop is very useful in the study of phase transition at finite temperature. The “condensate” of Polyakov loop serves as the order parameter of the confinement-deconfinement transition in the pure Yang-Mills theory.

To relate the fundamental quark confinement with the Polyakov loop it is intuitive to consider the free energy of a single static color charge, i.e., a quark

with infinite mass [1]

$$\begin{aligned} e^{-F_q/T} &= \text{Tr}_q e^{-H/T} / \text{Tr} e^{-H/T} \\ &= \frac{\sum_n \langle \Psi_n(1 \text{ quark}) | e^{-H/T} | \Psi_n(1 \text{ quark}) \rangle}{\sum_n \langle \Psi_n(0 \text{ quark}) | e^{-H/T} | \Psi_n(0 \text{ quark}) \rangle} \end{aligned} \quad (\text{A.3})$$

From the view point of path integral formalism the numerator is just an infinitely heavy quark propagating from  $(0, \vec{x})$  to  $(1/T, \vec{x})$ . Considering the kinetic part suppression due to the large mass the only contribution should come from the gauge field term which is equivalent to the Polyakov loop up to a constant

$$e^{-F_q/T} \sim \langle \text{Tr} L \rangle \quad (\text{A.4})$$

Obviously the quark confinement, which corresponds to  $F_q = +\infty$ , will induce  $\langle \text{Tr} L \rangle = 0$ . Otherwise  $\langle \text{Tr} L \rangle = 1$  if the quark is totally free. In this sense the Polyakov loop could be treated as a order parameter for the confinement deconfinement transition in the pure Yang-Mills theory. And it is also apparent that the intension of confinement is much more than the condensate of Polyakov loop. More information could be revealed by studying the topological details of it.

In the fundamental representation at spatial infinity up to a global transformation [20, 21]

$$L = \text{diag}(e^{2\pi i \mu_1}, e^{2\pi i \mu_2}, \dots, e^{2\pi i \mu_N}) \quad (\text{A.5})$$

Generators of  $SU(N)$  group are all traceless, so eigenvalues should satisfy

$$\mu_1 + \mu_2 + \dots + \mu_N = 0 \quad (\text{A.6})$$

With a global transformation we could order them as

$$\mu_1 \leq \mu_2 \leq \dots \leq \mu_N \leq \mu_{N+1} \equiv \mu_1 + 1 \quad (\text{A.7})$$

And in this paper the term holonomy will be used especially to call the set  $\{\mu_m | m = 1, 2, \dots, N\}$ . The holonomy is said to be trivial if  $L$  is in the center group  $Z_N$ . Because  $Z_N$  only has  $N$  one-dimensional complex irreducible representations, there are  $N$  choices for the trivial holonomy

$$\mu_m = \begin{cases} k/N - 1 & \text{when } m \leq k \\ k/N & \text{when } m > k \end{cases}$$

where  $k = 1, \dots, N$ . Without triviality constraint there would be lots of choices for the holonomy. A typical nontrivial one is the so-called ‘‘maximally non-trivial’’ one

$$\mu_m = -\frac{1}{2} - \frac{1}{2N} + \frac{m}{N} \quad (\text{A.8})$$

Obviously this is an equidistant one. And it gives  $\text{Tr} L = 0$

Phase transition often involves symmetry breaking or restoration. So it is for the confinement deconfinement transition. With the definition of the Polyakov loop we can see that its condensate is the order parameter for the center symmetry. In finite temperature field theory the operation of the center symmetry is defined through the twisted gauge transformation, which satisfies the boundary condition along the imaginary-time dimension

$$U(\vec{x}, x_4 + T^{-1}) = z U(\vec{x}, x_4) \quad (\text{A.9})$$

where  $z \in Z_N$  which is in the center of gauge group  $SU(N)$ . It could be checked that the Yang-Mills lagrangian density is invariant under the center symmetry transformation.

On the other hand under such a gauge transformation  $U(\tau, \vec{x})$ , the Polyakov loop transforms as

$$L[A_\mu^U] = L[U A_\mu U^\dagger + \frac{i}{g} U \partial_\mu U^\dagger] = U(\vec{x}, T^{-1}) L[A_\mu] U^\dagger(\vec{x}, 0) \quad (\text{A.10})$$

Using the boundary condition the trace of Polyakov loop should transform as

$$\text{Tr} L[A_\mu^U] = z \text{Tr} L[A_\mu] \quad (\text{A.11})$$

In confined phase the  $\langle \text{Tr} L \rangle = 0$  means the center symmetry is preserved. While in deconfined phase it becomes nonzero which means the symmetry breaking.

## B. The Perturbative Contribution to Holonomy Potential

Equilibrium state should be determined by the free energy

$$\begin{aligned} Z(T) &= \sum_n \langle n | e^{-H/T} P_{\text{phys}} | n \rangle \\ &= \int \mathcal{D}A \exp^{-S[A_\mu]} \\ &= e^{-F(T)/T} \end{aligned} \quad (\text{B.1})$$

Once the background configuration has been chosen

$$\begin{aligned} \vec{A} &= 0 \\ A_4 &= 2\pi T \text{diag}(\mu_1, \mu_2, \dots, \mu_N) \end{aligned} \quad (\text{B.2})$$

we can always do the 1-loop perturbative calculation above this mean field. The essential part is to complete the integration and summation for dressed propagators of gauge fields [46, 47].

$$\log \det(-D^2) = \sum_{j,k=1}^N \log \det\{-[\partial_\mu + 2\pi T(\mu_j - \mu_k)\delta_{4\mu}]^2\} - \log \det(-\partial^2) \quad (\text{B.3})$$



It could be seen that the longitudinal part of  $\delta A_i$ , which is the artifact of the gauge field, will cancel with the ghost part  $\delta A_4$  [47]. Taking the group measure into account and performing the Matsubara summation, the holonomy dependent part of the perturbative potential energy is related to the integration and summation as

$$\begin{aligned}
G &= \sum_{n=-\infty}^{+\infty} \int d^3p \log[(\omega_n + C)^2 + p^2] \\
&= \int d^3p \log(1 - 2\cos\beta C e^{-\beta p} + e^{-2\beta p}) \\
&= 8\pi \int p^2 dp \operatorname{Re}[\log(1 - e^{i\beta C} e^{-\beta p})] \\
&= \frac{8\pi}{\beta^3} (\operatorname{Li}_4(e^{i\beta C}) + \operatorname{Li}_4(e^{-i\beta C})) \\
&= \frac{8\pi}{\beta^3} \frac{(2\pi)^4}{24} B_4\left(\frac{(\beta C)_{\bmod 2\pi}}{2\pi}\right) \\
&= \frac{8\pi}{\beta^3} \frac{(2\pi)^4}{24} \left\{ \frac{1}{16} \left[ \left( 2\frac{(\beta C)_{\bmod 2\pi}}{2\pi} - 1 \right)^2 - 1 \right]^2 - \frac{1}{30} \right\} \\
&= \frac{\pi^5 T^3}{3} \left\{ \left[ \left( \left( \frac{C}{\pi T} \right)_{\bmod 2} - 1 \right)^2 - 1 \right]^2 - \frac{8}{15} \right\} \tag{B.4}
\end{aligned}$$

where holonomy independent parts have been omitted at the second equation. And the  $\operatorname{Li}_4(z)$  and  $B_4(z)$  are the polylogarithm function and Bernoulli polynomials of fourth order respectively. Here  $C$  represents different combinations  $\mu_j - \mu_k$  and  $\beta = T^{-1}$ .

Gathering all of contributions from different combinations  $C = \mu_j - \mu_k$ , up to a holonomy independent constant the perturbative potential energy for the  $SU(N)$  case is obtained as

$$P^{pert} = V \frac{(2\pi)^2 T^3}{3} \sum_{m>n}^N (\mu_m - \mu_n)^2 [1 - (\mu_m - \mu_n)]^2 \tag{B.5}$$

Especially for the  $SU(2)$  case there is only one term  $(\mu_2 - \mu_1)^2 [1 - (\mu_2 - \mu_1)]^2$  here. Using this formula the maximally non-trivial holonomy gives

$$\begin{aligned}
P^{pert, max} &= V \frac{(2\pi)^2 T^3}{3} \sum_{i=1}^{N-1} \frac{i^2}{N^2} \left(1 - \frac{i}{N}\right)^2 \\
&= V \frac{(2\pi)^2 T^3}{180} \frac{N^4 - 1}{N^2} \tag{B.6}
\end{aligned}$$

where the Faulhaber's formula are used to complete the summation  $\sum_{i=1}^N i^m$ . At this 1-loop level the perturbative potential energy has  $N$  minima corresponding to  $N$  elements of the center group. And the confining holonomy gives

larger potential energy than the trivial ones. This means at 1-loop level trivial holonomies, which indicate the deconfinement, are favored at arbitrary temperatures. Hence in order to achieve confinement at low temperature a more strict calculation is necessary with a topological non-trivial background configuration. The KvBLL Caloron is one of these choices.

### C. The KvBLL Caloron Solution

The caloron field with non-trivial holonomy discovered by Kraan and van Baal [17, 18] and independently by Lee and Lu [19] (therefore also known in the literature as the *KvBLL-caloron*), is a classical solution to the  $SU(N)$  Yang-Mills equations of motion in  $\mathbb{R}^3 \times S^1$ . It is a self-dual field with unit topological charge and most importantly, the  $A_4$  component can be gauged to be diagonal and constant at spatial infinity, which leads to a non-trivial Polyakov loop.

In the periodic gauge, the  $SU(2)$  KvBLL caloron field with period  $1/T$  is given by

$$A_\mu^{\text{KvBLL}} = \delta_{\mu 4} v \frac{\tau^3}{2} + \frac{\tau^3}{2} \bar{\eta}_{\mu\nu}^3 \partial_\nu \log \Phi + \frac{\Phi}{2} \text{Re} [(\bar{\eta}_{\mu\nu}^1 - i \bar{\eta}_{\mu\nu}^2) (\tau^1 + i \tau^2) (\partial_\nu + i v \delta_{\nu 4}) \tilde{\chi}], \quad (\text{C.1})$$

where

$$\begin{aligned} \hat{\psi} &= -\cos(2\pi T x_4) + \cosh(\bar{v}r) \cosh(vs) + \frac{r^2 + s^2 - \pi^2 \rho^4 T^2}{2rs} \sinh(\bar{v}r) \sinh(vs), \\ \psi &= \hat{\psi} + \frac{\pi^2 \rho^4 T^2}{rs} \sinh(\bar{v}r) \sinh(vs) + \pi \rho^2 T \left[ \frac{\sinh(vs) \cosh(\bar{v}r)}{s} \right. \\ &\quad \left. + \frac{\sinh(\bar{v}r) \cosh(vs)}{r} \right], \\ \tilde{\chi} &= \frac{\pi \rho^2 T}{\psi} \left[ e^{-2\pi i x_4} \frac{\sinh(vs)}{s} + \frac{\sinh(\bar{v}r)}{r} \right], \quad \Phi = \frac{\psi}{\hat{\psi}}. \end{aligned} \quad (\text{C.2})$$

Here,  $\bar{\eta}_{\mu\nu}^a \equiv \varepsilon_{\mu\nu}^a - \delta_\mu^a \delta_{\nu 4} + \delta_\nu^a \delta_{\mu 4}$  are the so called 't Hooft symbols,  $T$  the temperature and  $\tau^a$  the Pauli matrices. The meaning of the  $s$  and  $r$  variables will be explained shortly. From this expression, it is not hard to see that at spatial infinity, the fourth component is indeed diagonal and constant  $A_4|_{|\vec{x}| \rightarrow \infty} = v \frac{\tau^3}{2}$ . This asymptotic value is parametrized as  $v \equiv 2\pi T \nu$ , with  $\nu \in [0, 1]$  and analogously,  $\bar{v} = 2\pi T \bar{\nu}$  with  $\bar{\nu} = 1 - \nu$ . Thus, the trace of the Polyakov loop at spatial infinity has the non-trivial form

$$L_\infty \equiv \lim_{|\vec{x}| \rightarrow \infty} \frac{1}{2} \text{Tr} \mathcal{P} \exp \left( i \int_0^{1/T} d\tau A_4^{\text{KvBLL}} \right) = \cos(\pi \nu), \quad (\text{C.3})$$

	$M$	$\bar{M}$	$L$	$\bar{L}$
Electric charge	1	1	-1	-1
Magnetic charge	1	-1	-1	1
Action	$\nu \frac{8\pi^2}{g^2}$	$\nu \frac{8\pi^2}{g^2}$	$\bar{\nu} \frac{8\pi^2}{g^2}$	$\bar{\nu} \frac{8\pi^2}{g^2}$
Radius	$\frac{1}{v}$	$\frac{1}{v}$	$\frac{1}{\bar{v}}$	$\frac{1}{\bar{v}}$

Table C.1: Properties of the SU(2) (anti)dyons.

where  $\nu = \frac{1}{2}$  corresponds to maximal non-trivial holonomy ( $L_\infty = 0$ ) and  $\nu = 0$  trivial holonomy ( $L_\infty = 1$ ). Therefore,  $\nu$  is naturally called the *holonomy parameter*.

The anti-self-dual caloron or *anticaloron*  $\bar{A}_\mu$  with negative topological charge is easily obtained from Eq. (C.1) by

$$\begin{aligned}\bar{A}_4^{\text{KvBLL}}(\vec{x}, x_4) &= A_4^{\text{KvBLL}}(-\vec{x}, x_4) \\ \bar{A}_i^{\text{KvBLL}}(\vec{x}, x_4) &= -A_i^{\text{KvBLL}}(-\vec{x}, x_4).\end{aligned}\tag{C.4}$$

As expected, the KvBLL reduces to the Harrington-Shepard caloron [14] in the limit of trivial holonomy ( $\nu \rightarrow 0$  or  $\bar{\nu} \rightarrow 0$ ). Furthermore, it becomes a standard BPST instanton [13] of size  $\rho$  in the zero temperature limit.

One of the most important properties of this solution becomes relevant when  $\rho \gg 1/T$ . In this limit, the field is seen as composed of two constituent monopoles separated by a distance  $\pi\rho^2 T$ . As  $\rho \rightarrow \infty$ , the caloron becomes static and the monopoles are identified as the BPS type [48, 49] with unit, but opposite, electric and magnetic charges, therefore named *dyons* or in this context *instanton-dyons*.

(Anti)dyons are commonly known as (anti)self-dual static solutions of the Yang-Mills equations of motion with an adjoint scalar (Higgs) field. However, one can construct dyonic solutions in pure Yang-Mills theory with the condition of non-trivial holonomy, namely  $A_4|_{|\vec{x}| \rightarrow \infty} = v$ . For  $SU(2)$  there are four kinds of dyon solutions which following the usual convention in the literature are labeled  $M$  and  $L$  for the self-dual fields and  $\bar{M}$  and  $\bar{L}$  for the antiself-dual ones, referred to as *antidions* (see Table C.1). In the *hedgehog* gauge, the  $M$  fields have the form of the common BPS monopole solution (for more details on the derivation refer to [21, 50])

$$\begin{aligned}A_4^{M, \bar{M}} &= \mp n_a \left( v \coth(v|\vec{x}|) - \frac{1}{|\vec{x}|} \right) \frac{\tau^a}{2}, \\ A_i^{M, \bar{M}} &= \varepsilon_{aij} n_j \left( \frac{1}{|\vec{x}|} - \frac{v}{\sinh(v|\vec{x}|)} \right) \frac{\tau^a}{2},\end{aligned}\tag{C.5}$$

where  $n_a = x_a/|\vec{x}|$  and the (lower)upper sign corresponds to the (anti)self-dual solution.

If a gauge configuration consists of more than two dyons, it is inconvenient to superimpose them in this gauge, since we are interested in configurations where all dyons have the same  $A_4$  asymptotics at spatial infinity. This is achieved by using the matrices

$$S_+ = e^{-i\frac{\phi}{2}\tau^3} e^{i\frac{\theta}{2}\tau^2} e^{i\frac{\phi}{2}\tau^3} \quad \text{and} \quad S_- = -i\tau^2 S_+ = e^{i\frac{\phi}{2}\tau^3} e^{i\frac{\theta-\pi}{2}\tau^2} e^{i\frac{\phi}{2}\tau^3}, \quad (\text{C.6})$$

which satisfy the identity  $S_{\pm}(n_a\tau^a)S_{\pm}^{\dagger} = \pm\tau^3$ , and gauge-transform the dyon fields Eq. (C.5) as

$$A_{\mu}^{M,\bar{M}} \rightarrow S_{\mp} A_{\mu}^{M,\bar{M}} S_{\mp}^{\dagger} + iS_{\mp} \partial_{\mu} S_{\mp}^{\dagger}. \quad (\text{C.7})$$

In spherical coordinates, the dyon solutions in the new gauge take the form

$$A_4^{M,\bar{M}} = \frac{\tau^3}{2} \left( v \coth(v|\vec{x}|) - \frac{1}{|\vec{x}|} \right),$$

$$\pm A_i^{M,\bar{M}} = \begin{cases} A_r &= 0, \\ A_{\theta} &= \frac{v}{2 \sinh(v|\vec{x}|)} (\tau^1 \sin \phi + \tau^2 \cos \phi), \\ A_{\phi} &= \frac{v}{2 \sinh(v|\vec{x}|)} (\tau^1 \cos \phi - \tau^2 \sin \phi) + \frac{\tau^3}{2} \frac{\tan \frac{\theta}{2}}{|\vec{x}|}. \end{cases} \quad (\text{C.8})$$

One should notice first that now the  $A_4$  component is Abelian and equal for both  $M$  and  $\bar{M}$ . Moreover, we have introduced a singularity along the negative  $x_3$ -axis in  $A_{\phi}$ , a so called Dirac string which is merely a consequence of the gauge choice, hence the name *stringy gauge*.

The  $L$  and  $\bar{L}$  solutions are obtained from Eq. (C.8) by replacing  $v \rightarrow \bar{v}$  and apply two gauge transformations: first the time dependent  $U_1 = \exp(-i\pi T x_4 \tau^3)$  followed by a global rotation  $U_2 = \exp(i\pi\tau^2/2)$  [19, 51, 52]. As required, these will leave the asymptotics of  $A_4$  in the same form as for the  $M$  type solutions with the caveat that the spatial components are no longer static; however, in the large distance limit, neglecting exponentially small terms, the time dependent terms vanish and are no longer relevant in the scope of this article. The  $L$  type dyon fields in the stringy gauge thus are

$$A_4^{L,\bar{L}} = \frac{\tau^3}{2} \left( 2\pi T - \bar{v} \coth(\bar{v}|\vec{x}|) + \frac{1}{|\vec{x}|} \right),$$

$$\pm A_i^{L,\bar{L}} = \begin{cases} A_r &= 0, \\ A_{\theta} &= \frac{\bar{v}}{2 \sinh(\bar{v}|\vec{x}|)} [\tau^1 \sin(2\pi T x_4 - \phi) + \tau^2 \cos(2\pi T x_4 - \phi)], \\ A_{\phi} &= \frac{\bar{v}}{2 \sinh(\bar{v}|\vec{x}|)} [-\tau^1 \cos(2\pi T x_4 - \phi) + \tau^2 \sin(2\pi T x_4 - \phi)] \\ &\quad - \frac{\tau^3}{2} \frac{\tan \frac{\theta}{2}}{|\vec{x}|}. \end{cases} \quad (\text{C.9})$$

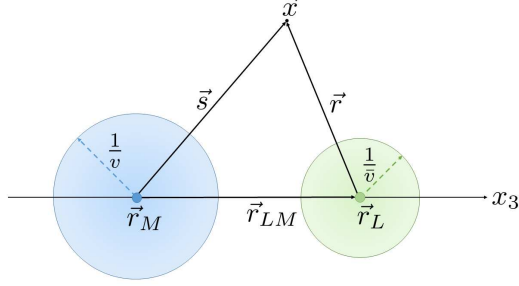


Figure C.1: Coordinates of the KvBLL caloron in terms of the center of mass positions of its constituent dyon fields.

Going back to the KvBLL field, the emergence of such configurations suggests to express the caloron in terms of the “constituent” dyon’s positions. The coordinates used to write the caloron in Eq. (C.1) are then the positions of the dyon’s center of mass denoted by  $\vec{r}_L$  and  $\vec{r}_M$ , the dyon separation  $r_{LM} \equiv |\vec{r}_L - \vec{r}_M| = \pi\rho^2 T$ , which for convenience is chosen to be along the  $x_3$ -axis (see Fig. C.1); i.e.  $\vec{r}_{LM} = r_{LM}\hat{e}_3$ , and the distances from the observation point  $\vec{x}$  to the dyon centers:  $\vec{s} = \vec{x} - \vec{r}_M$  and  $\vec{r} = \vec{x} - \vec{r}_L$ .

This monopole picture is more evident when looking at the caloron in the vicinity of one of its constituent dyons and far away from the other, namely at large separations. For instance, near the  $L$  dyon center and far away from the  $M$  dyon ( $s \gg 1/v$ ), the caloron field reduces to that of the  $L$  dyon, whose asymptotic behavior is given by (see Eq. (C.9))

$$A_4^{L,\bar{L}}|_{r \rightarrow \infty} = \frac{\tau^3}{2} \left( v + \frac{1}{r} \right) \quad \text{and} \quad A_\phi^{L,\bar{L}}|_{r \rightarrow \infty} = \mp \frac{\tau^3}{2} \frac{\tan \frac{\theta}{2}}{r}, \quad (\text{C.10})$$

where  $\phi$  and  $\theta$  are the polar and azimuthal angles in spherical coordinates centered at  $\vec{r}_L$ . The other components vanish in this limit. Analogously, near the  $M$  dyon and far away from the  $L$  ( $r \gg 1/\bar{v}$ ), the field is that of the  $M$  dyon with asymptotics (see Eq. (C.8))

$$A_4^{M,\bar{M}}|_{s \rightarrow \infty} = \frac{\tau^3}{2} \left( v - \frac{1}{s} \right) \quad \text{and} \quad A_\phi^{M,\bar{M}}|_{s \rightarrow \infty} = \pm \frac{\tau^3}{2} \frac{\tan \frac{\theta}{2}}{s}. \quad (\text{C.11})$$

Finally, in the limits  $s \gg 1/v$  and  $r \gg 1/\bar{v}$ , but not necessarily at large separations  $r_{LM}$ ; the KvBLL caloron field also becomes Abelian and takes the form

$$A_\mu^{\text{KvBLL}} = \frac{\tau^3}{2} (\delta_{\mu 4} v + \bar{\eta}_{\mu\nu}^3 \partial_\nu \log \Phi), \quad (\text{C.12})$$

where  $\Phi$  in this limit reduces to

$$\Phi = \frac{r + s + r_{LM}}{r + s - r_{LM}}. \quad (\text{C.13})$$

The only nonvanishing components of Eq. (C.12) are

$$\begin{aligned} A_4^{\text{KvBLL}} &= \frac{\tau^3}{2} \left( v + \frac{1}{r} - \frac{1}{s} \right), \\ A_\phi^{\text{KvBLL}} &= -\frac{\tau^3}{2} \left( \frac{1}{r} + \frac{1}{s} \right) \sqrt{\frac{(r_{LM} - r + s)(r_{LM} + r - s)}{(r_{LM} + r + s)(r + s - r_{LM})}}. \end{aligned} \quad (\text{C.14})$$

#### D. The Quantum Weight

In a similar fashion as it was done for the BPST instanton (at  $T = 0$ ) [53] and for the Harrington-Shepard caloron [46] (at  $T \neq 0$ ), it is of interest to calculate the contribution of small quantum oscillations of the KvBLL caloron to the Yang-Mills partition function

$$\mathcal{Z} = \int \mathcal{D}A_\mu e^{-S[A_\mu]} = \int \mathcal{D}A_\mu \exp \left[ -\frac{1}{2g^2} \int d^4x \text{Tr} F_{\mu\nu} F_{\mu\nu} \right]. \quad (\text{D.1})$$

In broad terms, this semiclassical procedure consists in taking the classical solution as a background field such that the gauge fields in the functional integral are

$$A_\mu(x) = A_\mu^{\text{KvBLL}}(x) + a(x), \quad (\text{D.2})$$

where  $a(x)$  is a small quantum fluctuation of the classical solution (the KvBLL field). Then expand the action around the saddle point up to the desired order in  $a_\mu$  and compute the functional integral.

In [54] Diakonov et al. obtained an analytic expression for the quantum weight of the  $SU(2)$  KvBLL caloron in the one-loop approximation. They showed that in the limit of large separation between the constituent dyons (in the temperature scale)  $r_{LM} \gg 1/T$ , it can be written as

$$\begin{aligned} \mathcal{Z}_{\text{KvBLL}} &= e^{-VP(\nu)} \int d^3r_L d^3r_M T^6 C 2\pi \left( \frac{8\pi^2}{g^2} \right)^4 \left( \frac{\Lambda_{\text{PV}} e^{\gamma_E}}{4\pi T} \right)^{\frac{22}{3}} \left( \frac{1}{Tr_{LM}} \right)^{\frac{5}{3}} \\ &\quad \times (1 + 2\pi T \nu \bar{\nu} r_{LM}) (1 + 2\pi T \nu r_{LM})^{\frac{8\nu}{3}-1} (1 + 2\pi T \bar{\nu} r_{LM})^{\frac{8\bar{\nu}}{3}-1}, \end{aligned} \quad (\text{D.3})$$

where  $P(\nu) = (4\pi^2/3)T^3\nu^2\bar{\nu}^2$  is the perturbative potential [46, 47] (see Appendix B),  $C \approx 1.03142$  is a combination of universal constants and the linear term in  $r_{LM}$  proportional to  $P''(\nu)$  from the exponential factor has been ignored in this work.

This expression can be further simplified in the approximation where the separation between dyons is much larger than their core sizes  $r_{LM} \gg \frac{1}{2\pi T\nu}, \frac{1}{2\pi T\bar{\nu}}$ ; taking the form

$$\mathcal{Z}_{\text{KvBLL}} = e^{-VP(\nu)} \int d^3r_L d^3r_M T^6 (2\pi)^{\frac{8}{3}} C \left( \frac{8\pi^2}{g^2} \right)^4 \left( \frac{\Lambda_{\text{PV}} e^{\gamma_E}}{4\pi T} \right)^{\frac{22}{3}} \nu^{\frac{8}{3}\nu} \bar{\nu}^{\frac{8}{3}\bar{\nu}}. \quad (\text{D.4})$$

To obtain Eq. (D.3), one has to calculate the invariant measure of the moduli space metric of the caloron field denoted as  $\sqrt{\det(g)}$ . In the general case of  $SU(N)$ , this is shown to be exactly equal to the determinant of a  $N \times N$  matrix  $\hat{G}$  [20, 55], which for  $SU(2)$  is given by

$$\sqrt{\det(g)} = \det(\hat{G}) \quad \text{where} \quad \hat{G} = \begin{pmatrix} 4\pi\bar{\nu} + \frac{1}{Tr_{LM}} & -\frac{1}{Tr_{LM}} \\ -\frac{1}{Tr_{LM}} & 4\pi\nu + \frac{1}{Tr_{LM}} \end{pmatrix}, \quad (\text{D.5})$$

which in the limit of large dyon separation reduces to  $\det(\hat{G}) \approx 16\pi^2\nu\bar{\nu}$ , and thus the partition function Eq. (D.4) is rewritten as

$$\begin{aligned} \mathcal{Z}_{\text{KvBLL}} = e^{-VP(\nu)} \int d^3r_L d^3r_M T^6 \frac{(2\pi)^{\frac{2}{3}}}{4} C \det(\hat{G}) \left( \frac{8\pi^2}{g^2} \right)^4 \left( \frac{\Lambda_{\text{PV}} e^{\gamma_E}}{4\pi T} \right)^{\frac{22}{3}} \\ \times \nu^{\frac{8}{3}\nu-1} \bar{\nu}^{\frac{8}{3}\bar{\nu}-1}. \end{aligned} \quad (\text{D.6})$$

The factor  $\left( \frac{\Lambda_{\text{PV}} e^{\gamma_E}}{4\pi T} \right)^{\frac{22}{3}}$ , appears from the running of the coupling constant  $g$ , in the Pauli-Villars regularization scheme. Namely

$$\left( \frac{\Lambda}{T} \right)^{\frac{22}{3}} = e^{-\frac{8\pi^2}{g^2(T)}}, \quad (\text{D.7})$$

where we have absorbed all constants into  $\Lambda$ . At the one loop calculation, the  $g^{-8}$  coupling in Eq. (D.10) is not renormalized; however, a two loop improvement (ignoring the effects on  $P(\nu)$ ) will give

$$\left( \frac{8\pi^2}{g^2} \right)^4 \left( \frac{\Lambda}{T} \right)^{\frac{22}{3}} \rightarrow \left( \frac{8\pi^2}{g^2(T)} \right)^4 e^{-\frac{8\pi^2}{g^2(T)}} h(T/\Lambda), \quad (\text{D.8})$$

where

$$h(T/\Lambda) = \exp \left\{ -\frac{34}{11} \log \left[ 2 \log \left( \frac{T}{\Lambda} \right) \right] + \frac{510}{1331} \frac{\log \left[ \frac{22}{3} \log \left( \frac{T}{\Lambda} \right) \right]}{\log \left( \frac{T}{\Lambda} \right)} \right\}. \quad (\text{D.9})$$

As an approximation, one can include the two loop improvement by substituting Eq. (D.8) and absorb the rest of the constant factors into a parameter  $\Gamma$  which is modulated in the simulation and fixed to be  $\Gamma \approx 0.119$ .

Finally, the caloron quantum weight takes the form

$$\begin{aligned}\mathcal{Z}_{\text{KvBLL}} &= e^{-VP(\nu)} \int d^3r_L d^3r_M \det(\hat{G}) T^6 \Gamma^2 S^4 e^{-S} \nu^{\frac{8}{3}\nu-1} \bar{\nu}^{\frac{8}{3}\bar{\nu}-1} \\ &= e^{-VP(\nu)} \int (d^3r_L f_L) (d^3r_M f_M) T^6 \det(\hat{G})\end{aligned}\quad (\text{D.10})$$

with

$$f_M = \Gamma S^2 e^{-\nu S} \nu^{\frac{8\nu}{3}-1}, \quad f_L = \Gamma S^2 e^{-\bar{\nu} S} \bar{\nu}^{\frac{8\bar{\nu}}{3}-1} \quad (\text{D.11})$$

the respective dyon fugacities and the instanton action

$$S(T) = \frac{8\pi^2}{g^2(T)} = \frac{22}{3} \log\left(\frac{T}{\Lambda}\right). \quad (\text{D.12})$$

## References

- [1] J. Greensite, Lect. Notes Phys. **821**, 1 (2011). doi:10.1007/978-3-642-14382-3
- [2] G. 't Hooft, Nucl. Phys. B **190**, 455 (1981). doi:10.1016/0550-3213(81)90442-9
- [3] Y. Nambu, Phys. Rev. D **10**, 4262 (1974). doi:10.1103/PhysRevD.10.4262
- [4] S. Mandelstam, Phys. Rept. **23**, 245 (1976). doi:10.1016/0370-1573(76)90043-0
- [5] G. Ripka, Lect. Notes Phys. **639**, 1 (2004) doi:10.1007/b94800 [hep-ph/0310102].
- [6] J. Liao and E. Shuryak, Phys. Rev. C **75**, 054907 (2007); Phys. Rev. Lett. **101**, 162302 (2008); Phys. Rev. Lett. **109**, 152001 (2012).
- [7] M. N. Chernodub and V. I. Zakharov, Phys. Rev. Lett. **98**, 082002 (2007) doi:10.1103/PhysRevLett.98.082002 [hep-ph/0611228].
- [8] A. D'Alessandro and M. D'Elia, Nucl. Phys. B **799**, 241 (2008) doi:10.1016/j.nuclphysb.2008.03.002 [arXiv:0711.1266 [hep-lat]].
- [9] C. Bonati and M. D'Elia, Nucl. Phys. B **877**, 233 (2013) doi:10.1016/j.nuclphysb.2013.10.004 [arXiv:1308.0302 [hep-lat]].
- [10] J. Liao and E. Shuryak, Phys. Rev. Lett. **102**, 202302 (2009) doi:10.1103/PhysRevLett.102.202302 [arXiv:0810.4116 [nucl-th]].



- [11] C. Ratti and E. Shuryak, Phys. Rev. D **80**, 034004 (2009) doi:10.1103/PhysRevD.80.034004 [arXiv:0811.4174 [hep-ph]].
- [12] J. Xu, J. Liao and M. Gyulassy, Chin. Phys. Lett. **32**, no. 9, 092501 (2015); JHEP 1602, 169 (2016) [arXiv:1508.00552 [hep-ph]].
- [13] A. A. Belavin, A. M. Polyakov, A. S. Schwartz and Y. S. Tyupkin, Phys. Lett. B **59**, 85 (1975). doi:10.1016/0370-2693(75)90163-X
- [14] B. J. Harrington and H. K. Shepard, Phys. Rev. D **17**, 2122 (1978). doi:10.1103/PhysRevD.17.2122
- [15] T. Schfer and E. V. Shuryak, Rev. Mod. Phys. **70**, 323 (1998) doi:10.1103/RevModPhys.70.323 [hep-ph/9610451].
- [16] D. Diakonov, Prog. Part. Nucl. Phys. **51**, 173 (2003) doi:10.1016/S0146-6410(03)90014-7 [hep-ph/0212026].
- [17] T. C. Kraan and P. van Baal, Nucl. Phys. B **533**, 627 (1998) doi:10.1016/S0550-3213(98)00590-2 [hep-th/9805168].
- [18] T. C. Kraan and P. van Baal, Phys. Lett. B **435**, 389 (1998) doi:10.1016/S0370-2693(98)00799-0 [hep-th/9806034].
- [19] K. M. Lee and C. h. Lu, Phys. Rev. D **58**, 025011 (1998) doi:10.1103/PhysRevD.58.025011 [hep-th/9802108].
- [20] D. Diakonov and V. Petrov, Phys. Rev. D **76**, 056001 (2007) doi:10.1103/PhysRevD.76.056001 [arXiv:0704.3181 [hep-th]].
- [21] D. Diakonov, Nucl. Phys. Proc. Suppl. **195**, 5 (2009) doi:10.1016/j.nuclphysbps.2009.10.010 [arXiv:0906.2456 [hep-ph]].
- [22] P. Gerhold, E.-M. Ilgenfritz and M. Muller-Preussker, Nucl. Phys. B **760**, 1 (2007) doi:10.1016/j.nuclphysb.2006.10.003 [hep-ph/0607315].
- [23] E. Shuryak and T. Sulejmanpasic, Phys. Lett. B **726**, 257 (2013) doi:10.1016/j.physletb.2013.08.014 [arXiv:1305.0796 [hep-ph]].
- [24] P. Faccioli and E. Shuryak, Phys. Rev. D **87**, no. 7, 074009 (2013) doi:10.1103/PhysRevD.87.074009 [arXiv:1301.2523 [hep-ph]].
- [25] R. Larsen and E. Shuryak, Nucl. Phys. A **950**, 110 (2016) doi:10.1016/j.nuclphysa.2016.03.013 [arXiv:1408.6563 [hep-ph]].
- [26] R. Larsen and E. Shuryak, Phys. Rev. D **92**, no. 9, 094022 (2015) doi:10.1103/PhysRevD.92.094022 [arXiv:1504.03341 [hep-ph]].
- [27] R. Larsen and E. Shuryak, Phys. Rev. D **93**, no. 5, 054029 (2016) doi:10.1103/PhysRevD.93.054029 [arXiv:1511.02237 [hep-ph]].

- [28] Y. Liu, E. Shuryak and I. Zahed, Phys. Rev. D **92**, no. 8, 085006 (2015) doi:10.1103/PhysRevD.92.085006 [arXiv:1503.03058 [hep-ph]].
- [29] Y. Liu, E. Shuryak and I. Zahed, Phys. Rev. D **92**, no. 8, 085007 (2015) doi:10.1103/PhysRevD.92.085007 [arXiv:1503.09148 [hep-ph]].
- [30] F. Bruckmann, S. Dinter, E. M. Ilgenfritz, M. Muller-Preussker and M. Wagner, Phys. Rev. D **79**, 116007 (2009) doi:10.1103/PhysRevD.79.116007 [arXiv:0903.3075 [hep-ph]].
- [31] B. Svetitsky and L. G. Yaffe, Nucl. Phys. B **210**, 423 (1982). doi:10.1016/0550-3213(82)90172-9.
- [32] R. Fiore, F. Gliozzi and P. Provero, Phys. Rev. D **58**, 114502 (1998) doi:10.1103/PhysRevD.58.114502 [hep-lat/9806017].
- [33] J. Engels, S. Mashkevich, T. Scheideler and G. Zinovev, Phys. Lett. B **365**, 219 (1996) doi:10.1016/0370-2693(95)01280-X [hep-lat/9509091].
- [34] J. Engels, J. Fingberg and M. Weber, Nucl. Phys. B **332**, 737 (1990). doi:10.1016/0550-3213(90)90010-B
- [35] J. Engels, J. Fingberg and D. E. Miller, Nucl. Phys. B **387**, 501 (1992). doi:10.1016/0550-3213(92)90171-7
- [36] M. Teper, Phys. Lett. B **313**, 417 (1993). doi:10.1016/0370-2693(93)90012-7
- [37] M. Caselle and M. Hasenbusch, Nucl. Phys. B **470**, 435 (1996) doi:10.1016/0550-3213(96)00161-7 [hep-lat/9511015].
- [38] A. Pelissetto and E. Vicari, Phys. Rept. **368**, 549 (2002) doi:10.1016/S0370-1573(02)00219-3 [cond-mat/0012164].
- [39] S. Digal, S. Fortunato and P. Petreczky, Phys. Rev. D **68**, 034008 (2003) doi:10.1103/PhysRevD.68.034008 [hep-lat/0304017].
- [40] S. Nadkarni, Phys. Rev. D **34**, 3904 (1986). doi:10.1103/PhysRevD.34.3904
- [41] D. Smith, A. Dumitru, R. Pisarski and L. von Smekal, Phys. Rev. D **88**, no. 5, 054020 (2013) doi:10.1103/PhysRevD.88.054020 [arXiv:1307.6339 [hep-lat]].
- [42] C. Borgs, Nucl. Phys. B **261**, 455 (1985). doi:10.1016/0550-3213(85)90582-6
- [43] E. Manousakis and J. Polonyi, Phys. Rev. Lett. **58**, 847 (1987). doi:10.1103/PhysRevLett.58.847
- [44] G. S. Bali, J. Fingberg, U. M. Heller, F. Karsch and K. Schilling, Phys. Rev. Lett. **71**, 3059 (1993) doi:10.1103/PhysRevLett.71.3059 [hep-lat/9306024].

- [45] L. Karkkainen, P. Lacock, D. E. Miller, B. Petersson and T. Reisz, Phys. Lett. B **312**, 173 (1993) doi:10.1016/0370-2693(93)90506-D [hep-lat/9306015].
- [46] D. J. Gross, R. D. Pisarski and L. G. Yaffe, Rev. Mod. Phys. **53**, 43 (1981). doi:10.1103/RevModPhys.53.43
- [47] N. Weiss, Phys. Rev. D **24**, 475 (1981). doi:10.1103/PhysRevD.24.475
- [48] E. B. Bogomolny, Sov. J. Nucl. Phys. **24**, 449 (1976) [Yad. Fiz. **24**, 861 (1976)].
- [49] M. K. Prasad and C. M. Sommerfield, Phys. Rev. Lett. **35**, 760 (1975). doi:10.1103/PhysRevLett.35.760
- [50] D. Diakonov and V. Petrov, Phys. Rev. D **67**, 105007 (2003) doi:10.1103/PhysRevD.67.105007 [hep-th/0212018].
- [51] K. M. Lee and P. Yi, Phys. Rev. D **56**, 3711 (1997) doi:10.1103/PhysRevD.56.3711 [hep-th/9702107].
- [52] K. M. Lee, Phys. Lett. B **426**, 323 (1998) doi:10.1016/S0370-2693(98)00283-4 [hep-th/9802012].
- [53] G. 't Hooft, Phys. Rev. D **14**, 3432 (1976) Erratum: [Phys. Rev. D **18**, 2199 (1978)]. doi:10.1103/PhysRevD.18.2199.3, 10.1103/PhysRevD.14.3432
- [54] D. Diakonov, N. Gromov, V. Petrov and S. Slizovskiy, Phys. Rev. D **70**, 036003 (2004) doi:10.1103/PhysRevD.70.036003 [arXiv:hep-th/0404042].
- [55] D. Diakonov and N. Gromov, Phys. Rev. D **72**, 025003 (2005) doi:10.1103/PhysRevD.72.025003 [hep-th/0502132].